Article

Developmental Cell

Detection of surface forces by the cell-wall mechanosensor Wsc1 in yeast

Graphical abstract

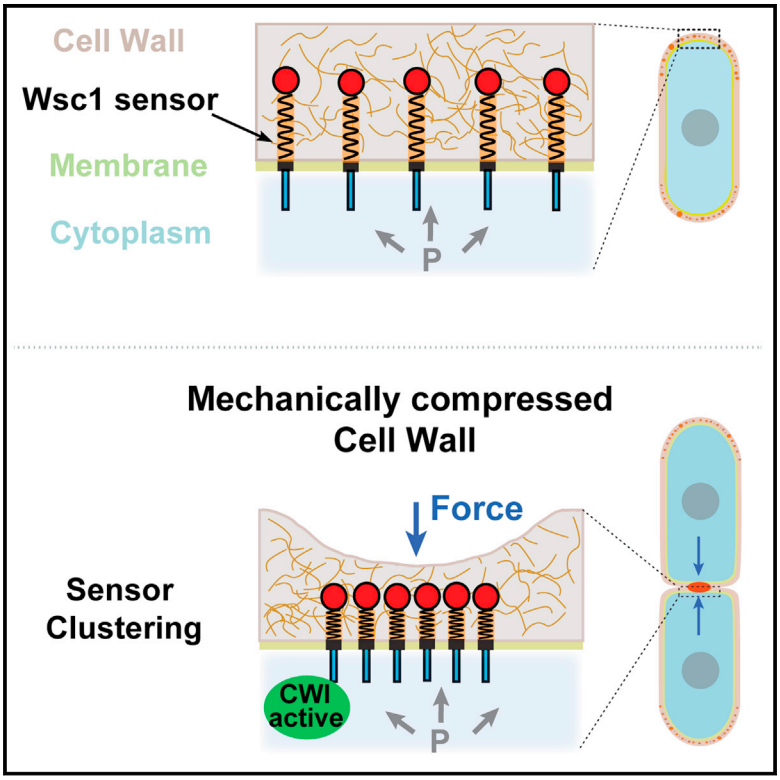

Authors

Ramakanth Neeli-Venkata, Celia Municio Diaz, Ruben Celador, Yolanda Sanchez, Nicolas Minc

Correspondence

nicolas.minc@ijm.fr

In brief

Neeli-Venkata et al. report the formation of large clusters of the surface protein Wsc1 at sites where forces are applied onto the yeast cell wall. Wsc1 acts as a *bona fide* mechanosensor and functions to detect local values of surface mechanical stress and activate pathways which reinforce the cell wall.

Highlights

- The surface sensor Wsc1 forms large clusters at sites of cell-wall compression
- Wsc1 senses mechanical stress in a reversible and dose-dependent manner
- Mechanosensing is mediated by Wsc1 cell-wall-interacting extracellular domains
- Wsc1 detects forces through force-dependent modulation of its surface diffusivity

Neeli-Venkata et al., 2021, Developmental Cell *56*, 1–15
October 25, 2021
https://doi.org/10.1016/j.devcel.2021.09.024

CellPress

Please cite this article in press as: Neeli-Venkata et al., Detection of surface forces by the cell-wall mechanosensor Wsc1 in yeast, Developmental Cell (2021), https://doi.org/10.1016/j.devcel.2021.09.024

Developmental Cell

CellPress

Article

Detection of surface forces by the cell-wall mechanosensor Wsc1 in yeast

Ramakanth Neeli-Venkata,[1,2] Celia Municio Diaz,[1,2] Ruben Celador,[3] Yolanda Sanchez,[3] and Nicolas Minc[1,2,4,*]
[1]Université de Paris, CNRS, Institut Jacques Monod, 75006 Paris, France
[2]Equipe Labellisée LIGUE Contre le Cancer, Paris, France
[3]Instituto de Biología Funcional y Genómica, CSIC/Universidad de Salamanca and Departamento de Microbiología y Genética, Universidad de Salamanca, C/ Zacarías González, 37007 Salamanca, Spain
[4]Lead contact
*Correspondence: nicolas.minc@ijm.fr
https://doi.org/10.1016/j.devcel.2021.09.024

SUMMARY

Surface receptors of animal cells, such as integrins, promote mechanosensation by forming clusters as signaling hubs that transduce tensile forces. Walled cells of plants and fungi also feature surface sensors, with long extracellular domains that are embedded in their cell walls (CWs) and are thought to detect injuries and promote repair. How these sensors probe surface forces remains unknown. By studying the conserved CW sensor Wsc1 in fission yeast, we uncovered the formation of micrometer-sized clusters at sites of force application onto the CW. Clusters assembled within minutes of CW compression, in dose dependence with mechanical stress and disassembled upon relaxation. Our data support that Wsc1 accumulates to sites of enhanced mechanical stress through reduced lateral diffusivity, mediated by the binding of its extracellular WSC domain to CW polysaccharides, independent of canonical polarity, trafficking, and downstream CW regulatory pathways. Wsc1 may represent an autonomous module to detect and transduce local surface forces onto the CW.

INTRODUCTION

Cells experience a large range of tensile, compressive, or shear forces from their environment, which influence growth, migration, or differentiation (Vogel and Sheetz, 2006). In animal cells, forces are typically detected at the cell surface through specific classes of integral membrane receptors, such as integrins or cadherins, which interact with the extracellular matrix or neighboring cells (Kechagia et al., 2019; Ladoux and Mège, 2017). Those receptors are connected to downstream elements, including scaffolding proteins, kinases and phosphatases, and cytoskeletal components, which together allow forces to be detected, transmitted, and transduced into biochemical signals that initiate adaptive responses (Chen et al., 2017). One conserved feature of surface sensing stands in the formation of receptor clusters (Hartman and Groves, 2011). For surface mechanosensing, for instance, specific force sensors and receptors may maturate into large cluster assemblies in response to tensile forces (Changede and Sheetz, 2017; Galbraith et al., 2002). Their formation and maturation under force could implicate *cis-cis* interactions, reduced local diffusivity, or membrane trafficking pathways, all dependent on local surface forces (Moreno-Layseca et al., 2019; Paszek et al., 2009; Welf et al., 2012). The functional role of clustering includes larger force-bearing and detection, noise-reduction in mechanoperception, as well as the separation of sensing units that probe local forces around cells at an intermediate scale much larger than that of single molecules (Changede and Sheetz, 2017). Thus, surface-sensor clustering may constitute a generic modular feature for cellular mechanobiology.

Nonmotile walled cells, such as plant and fungal cells, also express surface sensors, which may primarily interact and monitor properties of their CWs (Hamann and Denness, 2011; Levin, 2011; Pérez et al., 2018; Wolf et al., 2012). Some of these have been shown to form natural clusters at specific cell-wall locations that could bear high mechanical stress, such as growth sites in yeasts or around plasmodesmata in plants cells (Kock et al., 2015; Vu et al., 2020). Yeasts and fungi, for instance, feature two conserved families of single-pass transmembrane CW sensors of the WSC-type (cell wall stress-responsive component) and MID-type (mating-induced death). In analogy to animal receptors, these sensors have ~60–80 nm long extracellular domains embedded into the CW that may probe surface stress and integrity (Elhasi and Blomberg, 2019; Kock et al., 2015). They function as upstream triggers of the cell-wall integrity (CWI) pathway and activate CW-associated Rho GTPases and/or the expression of CW repair genes through protein kinases C and the Pmk1 MAPK, in response to global stresses, such as those caused by heat or antifungal agents (Levin, 2011; Pérez et al., 2018). Sensors from both families share a similar architecture with a cytoplasmic C-terminal tail that mediate downstream signaling, followed by a single

Please cite this article in press as: Neeli-Venkata et al., Detection of surface forces by the cell-wall mechanosensor Wsc1 in yeast, Developmental Cell (2021), https://doi.org/10.1016/j.devcel.2021.09.024

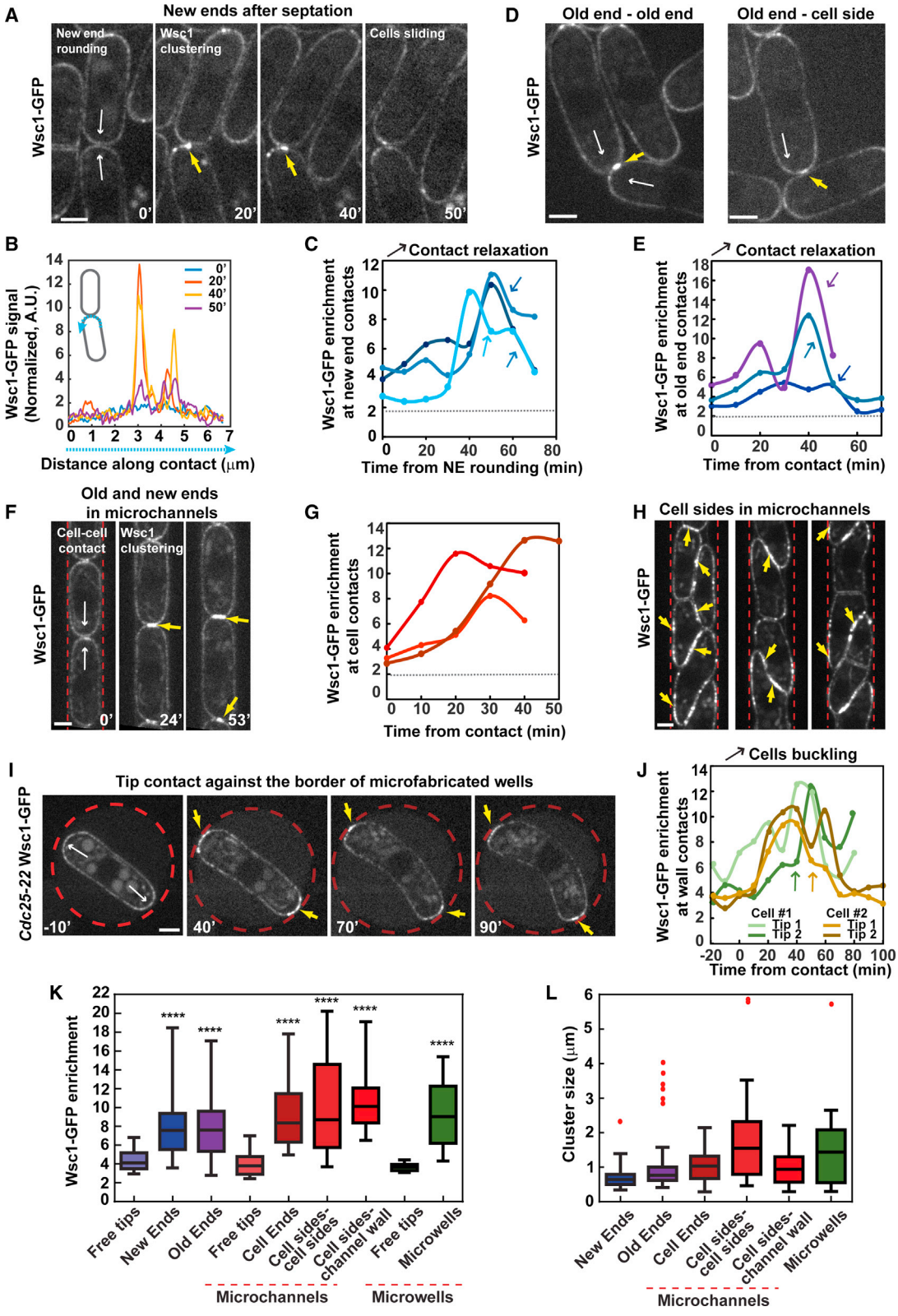

(legend on next page)

Please cite this article in press as: Neeli-Venkata et al., Detection of surface forces by the cell-wall mechanosensor Wsc1 in yeast, Developmental Cell (2021), https://doi.org/10.1016/j.devcel.2021.09.024

transmembrane domain (TMD), an O-mannosylated serine/threonine-rich region (STR), a head group, and a signal sequence. The head group of the WSC-type sensors is a conserved WSC cysteine-rich domain, and that of the MID-type is an N-glycosylated asparagine. These head groups are thought to interact with CW polysaccharides. For instance, WSC domains belong to C-type-lectin domain families that may bind carbohydrates through multiple weak interactions (Kock et al., 2015; Wawra et al., 2019). Pioneering studies using atomic force microscopy (AFM) on engineered polypeptides made of *S. cerevisiae* Wsc1 and Mid2 STR demonstrated that these domains can behave as nanosprings (expanding linearly with force) (Dupres et al., 2009). Therefore, CW sensors may embrace functional domains to interact with the CW, sense surface forces, and transduce them downstream. Accordingly, recent reports have directly implicated these sensors in CW mechanosensation and homeostasis (Banavar et al., 2018; Davì et al., 2018; Mishra et al., 2017). To date, however, whether and how CW nanosensors can directly probe CW mechanics or surface forces remains unknown (Kock et al., 2015).

We here report on the formation of large and stable micrometer-sized Wsc1 clusters at local sites of cell-cell contacts and CW compression in the fission yeast *Schizosaccharomyces pombe*. We establish the dose dependence of cluster formation on CW mechanical stress; their dynamics of assembly and disassembly in response to compression and relaxation, respectively; and their function in supporting CW integrity and survival. Our results suggest that Wsc1 probes surface mechanical stress and forms clusters at sites of enhanced stress through its extracellular WSC domain, independently of polarity and trafficking regulators and other canonical elements of the CWI pathway. We propose a reaction-diffusion model that allows Wsc1 to form clusters and autonomously detect local surface-compressive forces on the CW and transduce them to promote surface integrity.

RESULTS

Wsc1 forms clusters at sites of cell-cell contacts

Fission yeast features two important CW sensors, Wsc1 and Mtl2, which complement each other to support cell viability. Mtl2-GFP is localized all around the cell surface, while Wsc1-GFP is enriched at cell tips (Cruz et al., 2013). As previously reported in *S. cerevisiae*, we observed that Wsc1-GFP distribution around cell tips was nonuniform, with the clear appearance of little foci/clusters enriched in Wsc1 (Figure S1A) (Kock et al., 2015). Remarkably, by filming cells growing and dividing in standard agar pads, we made the serendipitous observation of the transient formation of bright and large micrometer-sized Wsc1-GFP clusters at sites of new-end-to-new-end contacts after cell division (Figure 1A; Videos S1 and S2). These clusters typically formed within tens of minutes after the completion of septation, when new ends round up and push onto each other due to turgor forces (Atilgan et al., 2015). Clusters were more prominent and stable in time when cells could not grow away from each other due to the presence of neighbors. In addition, upon cell rearrangement, cells frequently slid past each other, relaxing the contact and causing cluster disappearance within few minutes (Figures 1A–1C and S1B; Videos S1 and S2). Quantification of Wsc1-GFP enrichment, in representative time lapses revealed a local enrichment at contact sites that increased steadily over 30–40 min to reach values of about 10-fold and decayed upon cell rearrangement and contact relaxation on a time scale of 10–20 min. Local Wsc1-GFP clusters with similar appearance and disappearance kinetics were also observed when cells grew onto each other and contacted old end against old end or old end against cell sides, suggesting that they are not specific to septation (Figures 1B–1E; Videos S1 and S2). Finally, in several instances of cells contacting and sliding, Wsc1 clusters appeared to track the site of cell contact (Figure S1C). These observations suggest that Wsc1-GFP may dynamically sense and cluster at firm cell-cell contacts.

To enhance the formation and stability of cell contacts, we grew cells in linear, microfabricated PDMS (polydimethylsiloxane) channels (Haupt et al., 2018; Zegman et al., 2015). As cells grew ends against ends in the channels, they formed clusters that progressively increased in intensity and size. These clusters were seen in 81% of end contacts (n = 101 cells) at both old-ends and new-ends contacts and appeared more stable than in normal agar growth assay, presumably due to the absence of cell sliding and/or the more crowded environment. In addition,

Figure 1. The Wsc1 surface sensor forms micrometer-sized clusters at sites of cell-cell contacts

(A) Confocal midplane time lapse of WT cells expressing Wsc1-GFP growing and dividing on agar pads. Note the appearance of bright clusters at new-ends contact after septation (20′ and 40′), which disappear when cells slide apart and release pressure on the contact (50′). White arrows depict the direction of pressure-derived forces on the contact, and yellow arrows indicate Wsc1 clusters.

(B) Normalized fluorescence levels of Wsc1-GFP along the contact (blue dotted line in the inset), at each time point in (A).

(C) Dynamic of Wsc1-GFP enrichment in three representative pairs of dividing cells. The colored arrows indicate the moment when cells rearrange or slide apart and relax the contact. Dotted lines marks the reference value of enrichment of 2, corresponding to two apposed membranes.

(D) Wsc1-GFP clusters formed at an old-end-to-old-end or old-end-to-cell side contact.

(E) Wsc1-GFP enrichment dynamics at old end contacts in three representative cell pairs.

(F) Time lapse of wild-type cells expressing Wsc1-GFP grown in linear microchannels, demarked by red dotted lines.

(G) Wsc1-GFP enrichment dynamics at old- or new-end contacts in three representative cell pairs grown in microchannels.

(H) Examples of 3 individual microchannels in which cells have grown for longer periods (~5 h), adopting complex morphologies and packed arrangements, and resulting in Wsc1-GFP decorating large parts of cell sides even those pressed against channel walls.

(I) Single *cdc25-22* cells (at permissive temperature) expressing Wsc1-GFP grown in individual microwells form Wsc1 clusters when tips grow and press onto the microwell borders (indicated as a red dotted circle).

(J) Wsc1-GFP enrichment dynamics computed at the two tips of two representative single cells grown in microwells.

(K) Box plots of Wsc1-GFP enrichment in the different conditions presented in (1A–1I), compared with free growing tips with no contact for each condition (n = 16, 30, 30, 17, 36, 28, 28, 11, and 28 cells, respectively, from at least 3 independent experiments).

(L) Wsc1 cluster sizes in the different indicated conditions, with red dots corresponding to outliers in the distribution. Differences in Wsc1 enrichment between free tips and each condition were statistically confirmed by a two-tailed non-parametric Mann-Whitney test (****$p < 0.0001$).Error bars represent standard deviations. Scale bars, 2 μm.

Please cite this article in press as: Neeli-Venkata et al., Detection of surface forces by the cell-wall mechanosensor Wsc1 in yeast, Developmental Cell (2021), https://doi.org/10.1016/j.devcel.2021.09.024

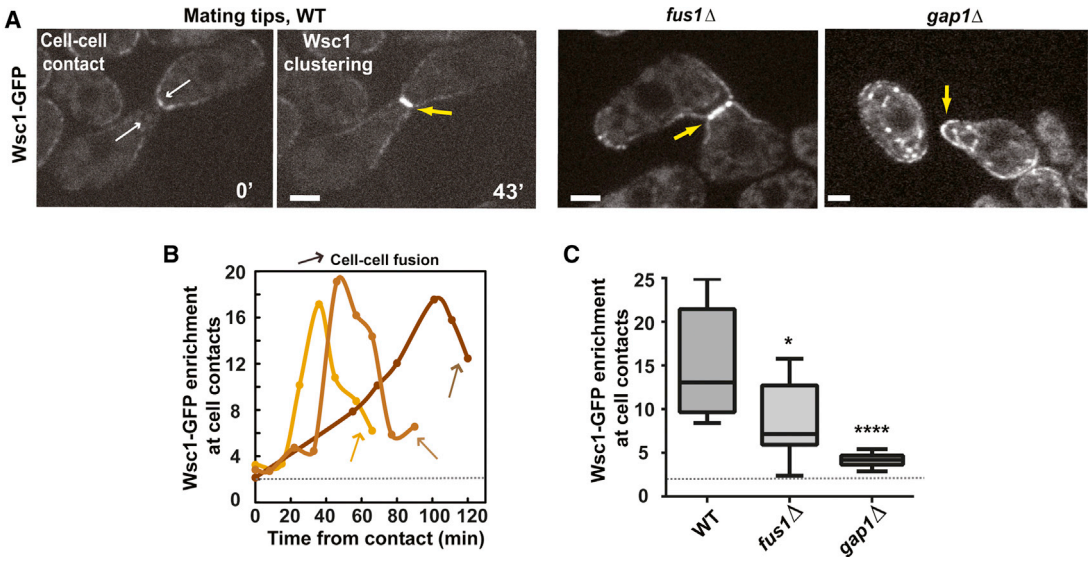

Figure 2. Wsc1 cluster formation at mating tip contacts

(A) Midplane confocal time lapse of WT cells expressing Wsc1-GFP undergoing mating (left). White arrows depict the direction of pressure-derived forces on the contact, and yellow arrows point to Wsc1 clusters. Images of *fus1Δ* and *gap1Δ* mutants expressing Wsc1-GFP (right).

(B) Dynamic of Wsc1-GFP enrichment in three representative pairs of WT mating cells. Time 0 corresponds to the first contact point, and arrows indicate the onset of CW opening prior to cell fusion. The dotted line in the graph corresponds to a reference value of enrichment of 2, corresponding to two apposed membranes.

(C) Wsc1-GFP enrichment at cell contacts in the indicated conditions (n = 13 cells for WT, 9 for *fus1Δ* and 12 for *gap1Δ*). For *gap1Δ* the enrichment was computed at shmoo tips and multiplied by 2 to compensate for the absence of partner cell. Results were compared by using a two-tailed non-parametric Mann-Whitney test. *$p < 0.05$, ****$p < 0.0001$. Error bars are standard deviations. Scale bars, 2 μm.

clusters appeared more prominent at flat cell-cell interfaces, indicative of higher mechanical stress on the contact (Figures 1F, 1G, and S1D–S1F; Video S3). Further, as cells grew and divided in channels over longer periods of times, they adopted abnormal triangular or trapezoidal shapes, thereby pushing onto each other or onto the channel walls on lateral sides (Haupt et al., 2018). Strikingly, in these cells, Wsc1-GFP decorated large parts of most lateral contacts, even those formed with channel walls (Figure 1H). Time-lapse imaging revealed that clusters could form *de novo* at the interface between a cell tip and the channel wall and were maintained at the contact site with the wall, translating toward the cell sides as tips grew away from the initial contact point. This recruitment at channel walls was nearly similar in microchannels pretreated with detergents to suppress nonspecific adhesion to PDMS (Colin et al., 2020), suggesting that they are not driven by putative protruding Wsc1 domains sticking to PDMS (Figures S1G, S2A, and S2B; Video S3). Clusters decorating lateral cell-cell contacts resulted from the progressive spreading of a cluster initially formed at a tip contact, due to the reorganization of polar growth and cells growing side-by-side and pressing onto each other along lateral contacts (Haupt et al., 2018) (Figure S1H; Video S3). Finally, 3D reconstitution did not reveal large-scale connection between individual clusters in the form of rings, for instance, suggesting that clusters act as local contact sensing units (Figure S1I).

To directly test if clusters can form independently of the presence of another cell, we grew isolated cells in single PDMS microwells(Minc et al., 2009b). When both tips elongated to contact and push against the borders of the well, they both formed clusters that became simultaneously brighter over time. Force exertion at cell tips was evident from cells buckling under the force of their own growth. Upon buckling, some clusters stayed intense at cell tips. In other cases, they relocated to a lateral location, as the contact with the chamber wall was maintained there and became broader and dimmer (Figures 1I and 1J; Video S4). Finally, in agreement with the formation of clusters against inert PDMS walls, Wsc1-GFP also clustered at contacts with a *wsc1Δ* cell (Figures S2C–S2E). Together, these results indicate that Wsc1 clustering may be triggered by local surface compression, independently of putative "*trans*" homotypic interactions between extracellular sensors from neighbor cells or general cell-to-cell signaling.

To compare these different conditions, we computed a distribution of Wsc1 enrichment in sets of representative images. Such quantification should yield a mean value of 2 for a contact-insensitive membrane factor, because of the presence of two apposed membranes at the contact site. Accordingly, the local enrichment of mCherry-Psy1, a single-pass transmembrane SNARE, independent of any CW signaling, was 1.86 ± 0.58 (mean ± SD) (Figures S2F–S2H). To normalize for the absence of another cell, enrichment of free growing tips, or those in contact with a PDMS wall, were multiplied by 2. This revealed a local enrichment of 4.06 ± 1.07 at free tips that reflected the polarized distribution of Wsc1-GFP. Enrichment at sites of surface compression was significantly higher, reaching values up to 20-fold, and were typically higher in microchannels, presumably because pressure on cell contacts may be stronger (Figure 1K). Cluster sizes varied between ~0.5 and 3 μm in width and were larger on larger contacts formed along lateral contacts in microchannels (Figures 1L and S1H). Finally, this analysis revealed no clustering phenotype for the other surface sensor, Mtl2, demonstrating it is specific to Wsc1 (Figures S2G and S2H).

Please cite this article in press as: Neeli-Venkata et al., Detection of surface forces by the cell-wall mechanosensor Wsc1 in yeast, Developmental Cell (2021), https://doi.org/10.1016/j.devcel.2021.09.024

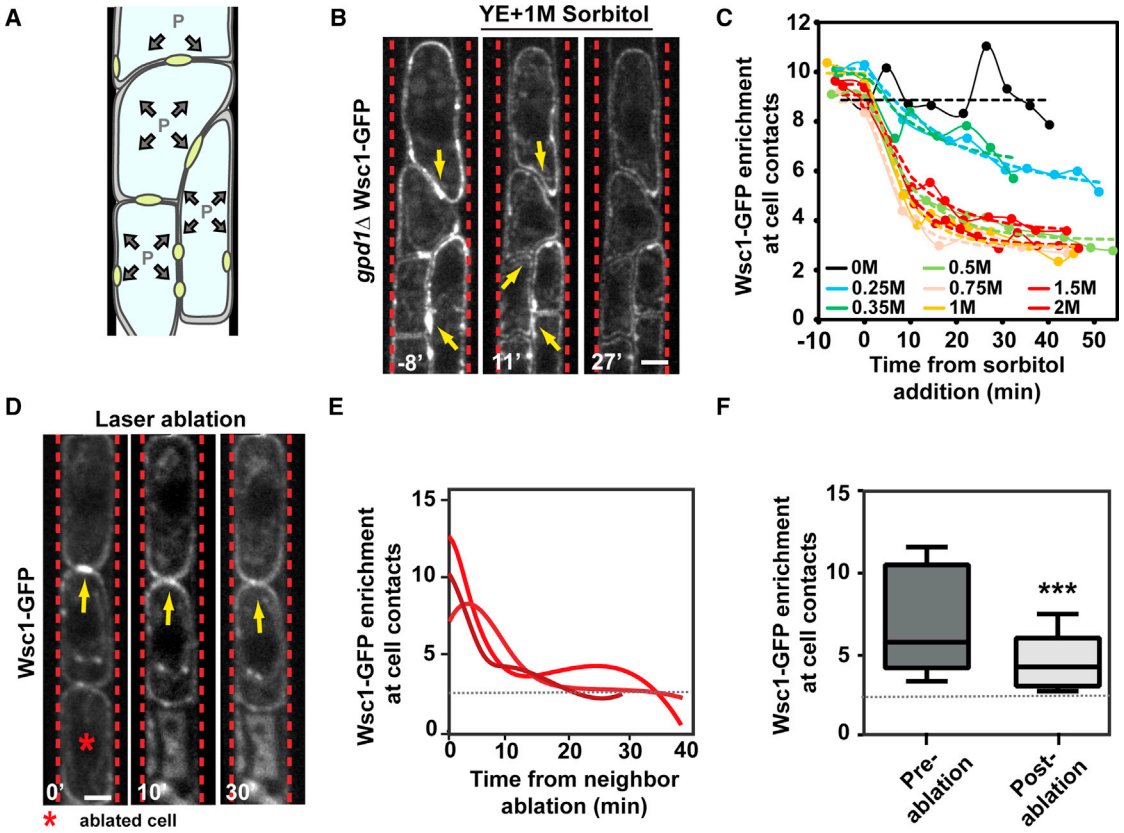

Figure 3. Turgor-derived mechanical stress in the cell wall promotes Wsc1 clustering

(A) Scheme representing cells pressing their cell wall due to turgor-pressure-derived stresses and forming Wsc1 clusters at sites of mechanical compression.

(B) Time lapse of *gpd1Δ* cells, defective in adapting internal turgor in response to hyperosmotic shocks, initially pressed onto each other through growth in microchannels and rinsed with 1-M sorbitol to reduce turgor. Note the disappearance of Wsc1 clusters when cells deflate and relax stress on the cell wall.

(C) Wsc1-GFP enrichment dynamics at cell contacts in response to treatment with different doses of sorbitol. Each point represents an average of 10–12 cells in different microchannels, and dotted lines are exponential fits of experimental data.

(D) Time lapse of cells in microchannels, in which laser ablation of one cell is used to relax pressure on neighbors, causing Wsc1 cluster disassembly. The red asterisk marks the ablated cell.

(E) Wsc1-GFP enrichment dynamics following laser ablation of neighbor cells in three representative experiments.

(F) Box plots of Wsc1-GFP enrichment 10 min before and 10 min after laser ablation of a neighbor (n = 5 cells). Results were compared using a two-tailed non-parametric Mann-Whitney test. ***$p < 0.001$. Error bars are standard deviations. Scale bars, 2 μm.

As another situation implicating cell-cell contacts, we also imaged Wsc1-GFP dynamics during mating. Wsc1-GFP was enriched at mating-tip projections, and was massively recruited when mating tips became apposed, reaching a local enrichment of up to ~20 fold in a time course of ~20–80 min. Wsc1 clusters disappeared during cell fusion, as apposed CWs became digested (Figures 2A and 2B; Video S5). Importantly, Wsc1 clusters still formed in mating pairs of *fus1Δ* cells, impaired in mating-specific polarized trafficking but reached an enrichment that was significantly smaller than in wild-type (WT) mating but closer to that found for interphase WT cell contacts (Dudin et al., 2015). In addition, *gap1Δ* cells, which form random mating projections without contacting partners, did not enrich Wsc1 at cell tips to these high levels (Figures 2A and 2C) (Imai et al., 1991; Merlini et al., 2018). Thus, Wsc1 clustering at mating tips may be driven by the contact of apposed CWs and further enhanced by mating-specific polarity machineries. All together, these data demonstrate that the Wsc1 CW sensor may dynamically sense and accumulate to local cell contacts where CWs are pressed.

Wsc1 clustering is triggered by mechanical stress in the cell wall

Fission yeast cells harbor high internal turgor pressure on the order of ~1.0–1.5 Mpa, which impart, large mechanical stress on the elastic CW (Abenza et al., 2015; Davì and Minc, 2015; Minc et al., 2009a). As cells grow and push onto each other, this stress may become enhanced locally, causing Wsc1 surface sensors to accumulate to cell contacts (Figure 3A). To test the role of mechanical stress, we first followed Wsc1-GFP clusters formed in WT cells in microchannels and rinsed with 2-M sorbitol to drastically reduce turgor . Cells rapidly deflated, causing a complete disappearance of Wsc1 clusters within tens of minutes. Rinsing back with normal media, caused cells to re-inflate and Wsc1-GFP to reaccumulate at the same location (Figures S3A and S3B). To circumvent turgor adaptation and to better compute a threshold in pressure values needed to maintain clusters, we performed deflation experiments with increasing doses of sorbitol in a *gpd1Δ* mutant background defective in turgor adaptation (Ohmiya et al., 1995). These assays revealed that clusters

Please cite this article in press as: Neeli-Venkata et al., Detection of surface forces by the cell-wall mechanosensor Wsc1 in yeast, Developmental Cell (2021), https://doi.org/10.1016/j.devcel.2021.09.024

disappeared with a time scale of ~20 min for all concentrations of sorbitol above 0.5 M. For concentrations below, the disappearance was much less pronounced (Figures 3B and 3C). These results estimate a threshold in turgor of ~0.4 to 0.6 MPa for maintaining Wsc1 clusters, similar to that needed to deform the CW and drive cell growth in these cells (Atilgan et al., 2015; Bonazzi et al., 2014; Haupt et al., 2018; Minc et al., 2009a).

Because sorbitol treatment could indirectly affect Wsc1 membrane localization, we also followed Wsc1 clusters and ablated neighboring cells to relax mechanical stress at cell contacts (Haupt et al., 2018). Following ablation, cells slowly separated, likely hindered by CW remnants of ablated cells, yielding to the progressive disassembly of Wsc1 clusters (Figures 3D–3F). Similarly, ablating one partner during mating yielded CW relaxation in the nonablated partner and cluster disappearance within a few minutes (Figures S3C and S3D). Together, these data directly suggest that Wsc1 forms reversible clusters at sites of enhanced mechanical stress in the CW, demonstrating that Wsc1 acts as a *bona fide* surface mechanosensor.

Mechanical stress in the CW depends on a balance between turgor values and the thickness of the CW. To assay the role of CW thickness in Wsc1 response, we first chemically thinned the CW by growing cells on agar pads supplemented with caspofungin, a drug that affects CW synthesis. This led to the formation of a very bright, single Wsc1 cluster at the site of new-end contacts that followed septation, even when cells were not restricted by neighboring cells. In 55% of cases, this clustering event was followed by the lysis of one or two of the daughter cells, indicative of thinner or weaker CWs (Figures 4A, 4B, and S3E). Dispersed bright clusters also appeared transiently at cell tips, preceding bulging plausibly reflecting thinner or softer CWs (Davì et al., 2018). Thus, chemically thinned or weakened CWs, which bear higher stress can recruit Wsc1 clusters.

To directly assay the dose-dependent impact of CW mechanical compression we next adapted a previous subresolution method, to compute the sum of the thickness of apposed CWs at sites of cell contacts (Davì et al., 2018, 2019). We mixed populations of cells expressing mCherry-Psy1 and Wsc1-GFP in microchannels and monitored contacts at the interfaces between differently labeled cells. Because Wsc1-GFP is a single-pass transmembrane protein tagged at its intracellular tail, like mCherry-Psy1, we fitted each membrane signal with a Gaussian, and computed the peak-to-peak distance to extract the sum of thicknesses of apposed CWs (Figure 4C). As controls, we verified that Wsc1-GFP signals gave similar values of mean CW thickness as GFP-psy1 in normal cells (Figure S4A). In addition, measurements obtained with Wsc1-GFP or with a nonclustering, membrane-associated domain tagged with BFP (RitC-BFP), expressed in the same cell, yielded nearly similar apposed CW thickness values (Figures S4B–S4D) (Vještica et al., 2020). Using this we monitored concomitant changes in apposed CW thicknesses and Wsc1 enrichments. As cells grew onto each other, the contact flattened and the sum of apposed CWs thickness changed from above ~300 nm, corresponding to the sum of normal CW thicknesses at cell tips (Davì et al., 2018), to values down to 150–200 nm, corresponding to a relative thinning of CWs of up to ~50%. This suggests that apposed CWs are submitted to compressive forces that cause them to thin with a rate likely determined by growth and divisions in the channel. Importantly, as CWs were more compressed, Wsc1-GFP clusters became more intense suggesting that progressive stress increase promotes further Wsc1 accumulation (Figures 4D and 4E). Conversely, by performing neighbor-ablation assays, CWs progressively relaxed yielding to the disassembly of Wsc1 clusters (Figures 4F–4G). Finally, the same analysis in mating cells showed that apposed CWs of mating partners could thin by up to ~80%, yielding more pronounced recruitment of Wsc1-GFP (Figures S4E and S4F). During mating, this overthinning is most likely partially accomplished by enzymatic digestion of apposed CWs in addition to pure mechanical thinning. Computing Wsc1-GFP enrichment as a function of CW thickness changes for all above mentioned conditions revealed a clear dose dependence of Wsc1 enrichment as a function of CW compression (Figure 4H). Although the geometry of contacts and the presence of multiple cells precludes a simple calculation of the precise stresses borne by CWs, rough estimates suggest that an increase of ~2× in local mechanical stress may drive a ~10× enrichment in Wsc1-GFP. Thus, although these data do not currently allow discerning if Wsc1 directly senses thickness, elastic strains, stresses, or other mechanical parameters, they strongly support a dose-dependent recruitment of Wsc1 sensors with compressive forces onto the CW.

Wsc1 may behave as an autonomous module to detect local CW mechanical stress

We sought to dissect mechanisms of Wsc1 clustering upon mechanical stress. In normally growing cells, Wsc1-GFP localizes to cell tips, at sites enriched in polarity factors, actin assembly, endo- and exocytosis, and CW remodeling regulators (Martin and Arkowitz, 2014). In addition, previous reports suggested that Wsc1 polar distribution is partially dependent on F-actin and is located to the only growing tip in monopolar mutants like *tea1Δ* and *tea4Δ* (Cruz et al., 2013). Building on our microchannels assay, where clusters are highly penetrant, and form at multiple sites around the cell surface—not only at cell tips—we first co-imaged active-Cdc42 (using the CRIB-GFP probe) as a general marker of polarity and actin assembly together with Wsc1-mCherry. When clusters formed at sites of tip-tip contacts, they co-localized with CRIB-GFP but were notably more focused than CRIB-GFP patches, accumulating at the precise site where CW contacts appeared flat (Figure S5A). However, in a significant number of cells, clusters also formed at a contact with a neighbor CW away from the growing tip and active-Cdc42 zones. Similar results were also obtained by co-imaging Wsc1 and the upstream regulator of polar growth and CW synthesis RFP-Bgs4 (Figure 5A). Thus, Wsc1 clusters forming at sites of local CW compression can be spatially uncoupled from polarity machineries.

We next screened a set of well-characterized conditions and mutants defective in polarity, endo- or exocytosis, actin assembly, and secretory vesicle trafficking (Figures 5B, 5C, and S5C–S5E). Factors implicated in polarity establishment at the new end, such as microtubules Mal3, Tea1, Tea4, or Pom1, were dispensable for Wsc1 clustering. Analyses of *end4Δ*, *myo1Δ*, and *wsp1Δ* mutants strongly defective in endocytosis, revealed no major defects or enhancement of Wsc1-GFP enrichment at compressed CWs. Importantly, in these endocytic mutants, Wsc1 was largely delocalized from cell tips in free-growing cells,

Please cite this article in press as: Neeli-Venkata et al., Detection of surface forces by the cell-wall mechanosensor Wsc1 in yeast, Developmental Cell (2021), https://doi.org/10.1016/j.devcel.2021.09.024

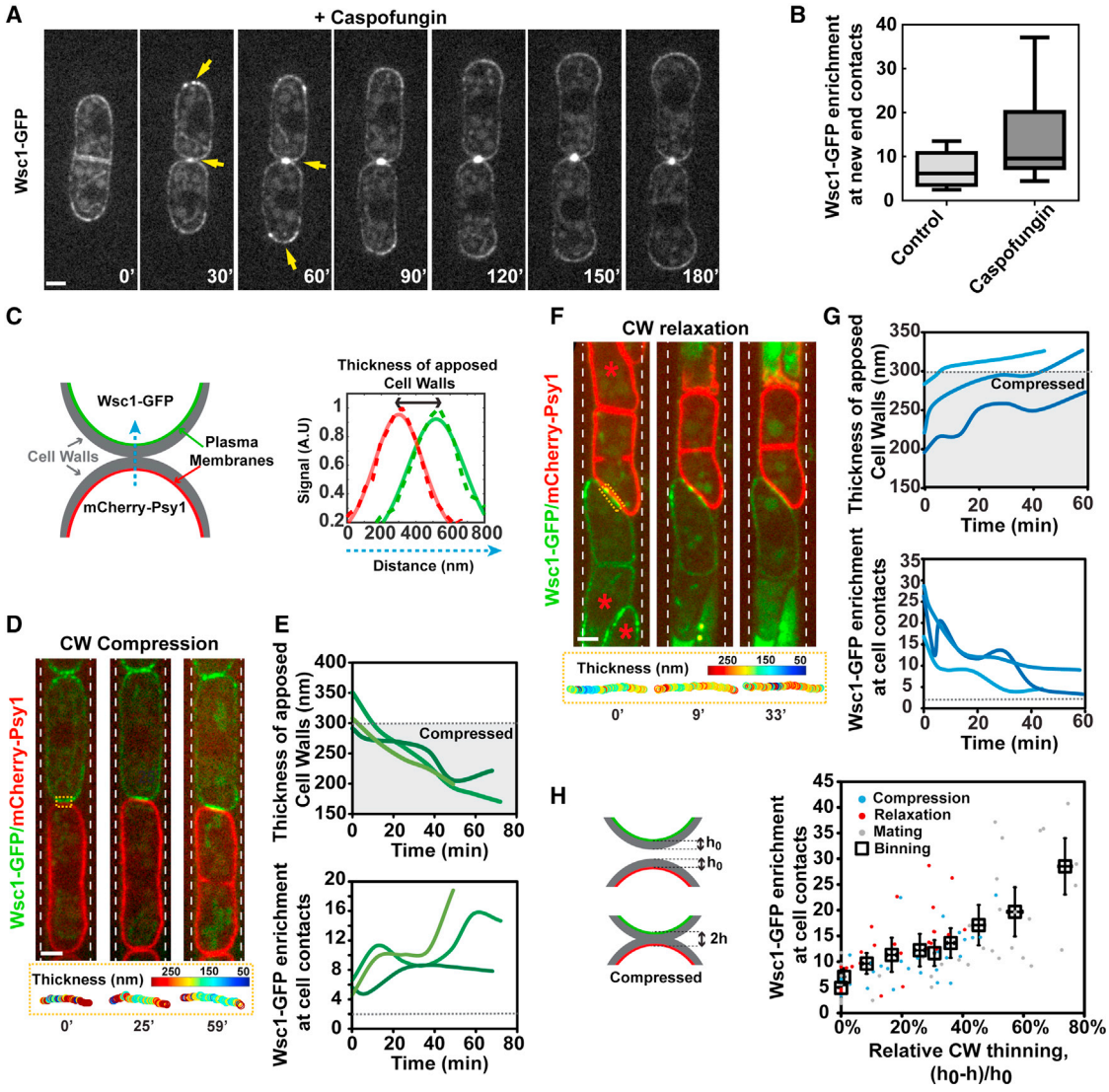

Figure 4. Compressive forces onto the cell wall trigger dose-dependent Wsc1 clustering

(A) Time lapse of a pair of WT cells expressing Wsc1-GFP in the presence of caspofungin. Note the bright single dot at the site of new-end contacts, and the multiple dots at cell tips preceding bulging.

(B) Quantification of Wsc1-GFP enrichment at new-end contacts in controls versus caspofungin treated cells (n = 12 and 9, respectively).

(C) Scheme representing the subresolution imaging method to compute the thickness of apposed cell walls from the peak signal of plasma membranes tagged with different fluorophores.

(D) Example of a cell expressing Wsc1-GFP that grows onto a cell expressing mCherry-Psy1 in microchannels with the thickness of CWs along the contact represented with a color map (bottom).

(E) Thickness evolution of apposed cell walls as cells grow onto each other in three exemplary cell pairs, and concomitant evolution of Wsc1-GFP enrichment at the contact. The gray zone in the thickness plot corresponds to a zone smaller than the sum of normal thicknesses of CWs in free cells.

(F) Example of a cell expressing Wsc1-GFP pressed against a cell expressing mCherry-Psy1 in microchannels, where the contact is relaxed by ablating neighbors (marked with a red asterisk) and computation of the thickness of CWs along the contact represented with a color map (bottom).

(G) Thickness evolution of apposed cell walls as cells separate and relax their cell walls at the contact due to neighbor ablation in three exemplary cell pairs and concomitant evolution of Wsc1-GFP enrichment at the contact.

(H) Wsc1-GFP enrichment plotted as a function of the relative thinning of apposed CWs with respect to free cells, for cells undergoing compression, relaxation in interphase, or during mating. The squares are bins of 10 individual measurements, with error bars representing standard deviations (n= 92 clusters in total). Scale bars, 2 μm.

suggesting that Wsc1 clustering at sites of CW mechanical stress does not require any prior tip localization. Similar clustering behavior was obtained in secretion mutants *exo70Δ* and *sec8-1*^{ts}, as well as in the formin *for3Δ* and myosin type V *myo52Δ* mutants, which are defective in secretory vesicle trafficking along actin cables. This suggests that cluster formation may predominantly emerge as a result of reaction-diffusion or flows along the plasma membrane and CW, rather than

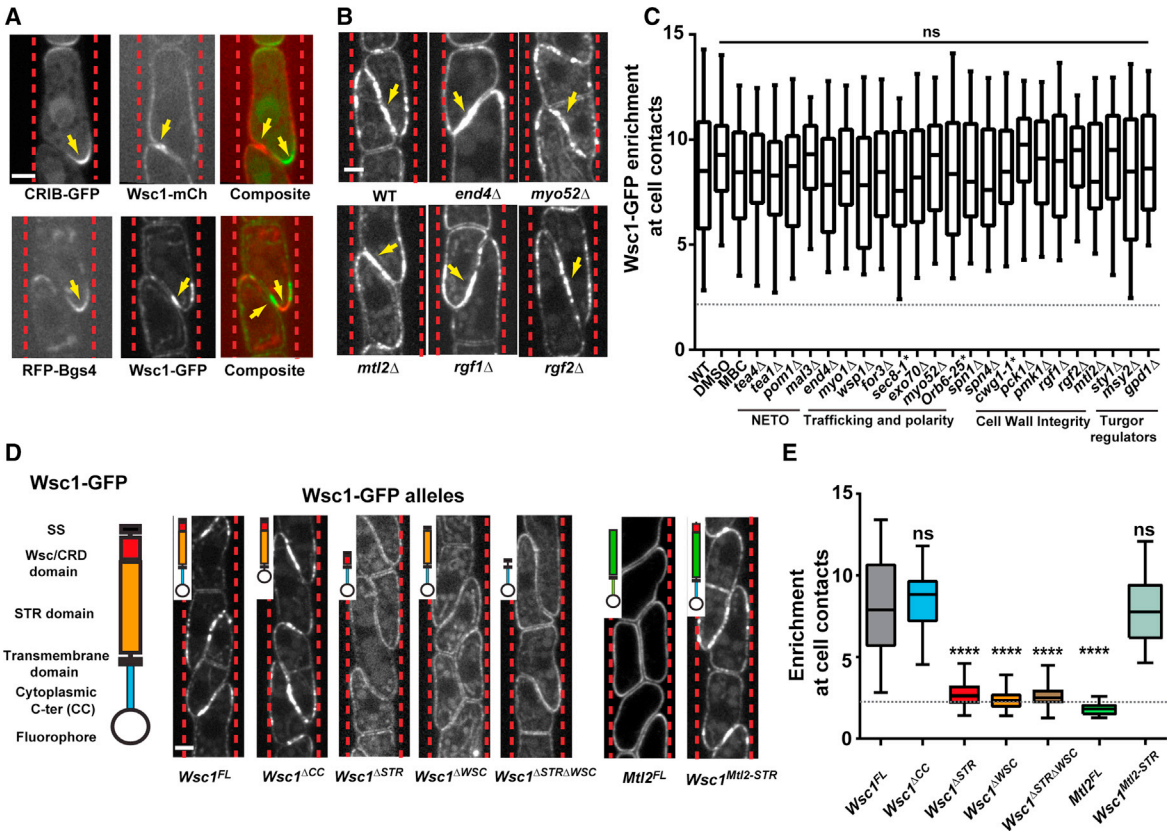

Figure 5. Force-dependent Wsc1 clustering is independent of downstream polarity, trafficking, and CW regulation but requires extracellular CW-interacting domains

(A) Co-imaging of active Cdc42 (CRIB-GFP) and Wsc1-mCherry clusters (top), and RFP-Bgs4 with Wsc1-GFP clusters (bottom) in cell pairs in microchannels.

(B) Representative images of Wsc1-GFP clusters in cell pairs in microchannels in the indicated mutants.

(C) Boxplots of Wsc1-GFP enrichment at sites of contacts in the indicated trafficking, polarity, and CWI mutants and alleles (n > 50 cells for each condition, from at least three independent experiments).

(D) Scheme representing the main functional Wsc1 domains and representative images of different tagged alleles lacking one or several of these domains, or with a domain swapped with the corresponding domain in Mtl2 (see insets) in microchannels.

(E) Box plots of GFP-tagged alleles enrichment at cell contacts in microchannels (*Wsc1* ^{FL}*-GFP* [full length], n = 65 cells; *Wsc1*$^{\Delta CC}$*-GFP*, n = 45; *Wsc1*$^{\Delta STR}$*-GFP*; n = 66; *Wsc1*$^{\Delta WSC}$ *-GFP*, n = 33; *Wsc1*$^{\Delta STR\Delta WSC}$*-GFP*, n = 87; *Mtl2* ^{FL}-GFP, n = 21, *Wsc1*$^{STR\text{-}Mtl2}$*-GFP*; n = 26). Results were compared using a two-tailed non-parametric Mann-Whitney test. n.s. $p > 0.05$, ****$p < 0.0001$. Error bars are standrad deviations. Scale bars, 2 μm.

recycling. Further, tests of the major septin mutants *spn1Δ* and *spn4Δ* indicated no role for these scaffold proteins in mediating or restricting lateral diffusion or flows of Wsc1 needed for cluster formation. Finally, an *orb6-25*^{ts} mutant defective in polar growth still formed clusters, confirming that Wsc1 does not rely on Cdc42-based polarity to form clusters at CW compression sites. These data suggest that Wsc1 can sense and accumulate to sites of local CW compression independently of canonical polarity and trafficking pathways.

Because Wsc1 is upstream of the CWI pathway, we also screened components of this pathway to test the contribution of putative positive feedbacks that could enrich Wsc1 clusters when the pathway is activated by surface forces (Figures 5B, 5C, and S5C–S5E) (Madrid et al., 2006; Pérez et al., 2018). Using a *cwg1-1* ^{ts} allele defective in CW synthesis, we first ruled out a major role for CW synthesis and remodeling in Wsc1 clustering. Also, null mutants in the protein kinase C, Pck1, and in the MAPK Pmk1 did not exhibit defects, suggesting no direct role for transcriptional responses. Similarly, upstream CWI GEFs Rgf1 and Rgf2, which act downstream of surface sensors to activate the Rho GTPase Rho1 for CW repair, did not exhibit notable defects in clustering. In addition, the other surface sensor, Mtl2, did not contribute to Wsc1 clustering, further supporting their independence in probing and transducing CW stress (Cruz et al., 2013). Finally, clusters also formed in *sty1Δ* and *gpd1Δ* mutants defective in turgor adaptation to hyper-osmotic conditions, or in *msy2Δ* defective in adaptation to hypo-osmotic conditions. This indicates that putative pressure adaptation may not contribute significantly to increased mechanical stress and Wsc1 clustering. Thus, downstream elements that regulate CW integrity and mechanical adaptation are not required for Wsc1 mechanosensation.

The CW-associated extracellular WSC domain is required for force sensing and clustering

We then generated fluorescently tagged and untagged Wsc1 alleles that lack one or several core functional domains: A *Wsc1*$^{\Delta CC}$ that lacks the cytoplasmic C-terminal tail, a *Wsc1*$^{\Delta TMD}$

Please cite this article in press as: Neeli-Venkata et al., Detection of surface forces by the cell-wall mechanosensor Wsc1 in yeast, Developmental Cell (2021), https://doi.org/10.1016/j.devcel.2021.09.024

that lacks the TMD, a *Wsc1*$^{\Delta STR}$ lacking the long STR "nanospring" extracellular domain, a *Wsc1*$^{\Delta WSC}$ that lacks the cysteine-rich WSC domain, and a *Wsc1*$^{\Delta STR\Delta WSC}$ that lacks all extracellular domains except for the signal sequence. Allele design followed sequence alignment with established alleles from *S. cerevisiae* Wsc1 (Philip and Levin, 2001), and all encoding constructs were integrated at the *wsc1*$^{+}$ locus.

Tagged and untagged alleles were viable, with no defects in cell size or morphology, but exhibited some low fraction (~5%) of cell death, similar to the null *wsc1Δ* mutant (Figure 7D) (Cruz et al., 2013). Except for the *Wsc1*$^{\Delta TMD}$*-GFP* allele which was completely intracellular, all alleles were still enriched at the plasma membrane, with *Wsc1*$^{\Delta WSC}$*-GFP* exhibiting the most pronounced localization to internal membranes, potentially reflecting a role of the WSC domain for sensor stability at the membrane or within the CW (Kock et al., 2015). Tagged alleles were also all localized to cell tips, with *Wsc1*$^{\Delta WSC}$*-GFP*, *Wsc1*$^{\Delta STR}$*-GFP*, and *Wsc1*$^{\Delta STR\Delta WSC}$*-GFP* exhibiting less polarized patterns, suggesting a partial function for extracellular domains in maintaining Wsc1 to the exact tips (Figures S5F–S5H). Using microchannel assays, we screened for putative clustering defects of these alleles. Remarkably, the *Wsc1*$^{\Delta CC}$*-GFP* lacking a large fraction of the cytoplasmic C-terminal tail, and thus presumably defective in downstream signal transduction was dispensable for clustering. This finding reinforces the notion that Wsc1 clustering occurs independently of downstream CWI signaling. In sharp contrast, *Wsc1*$^{\Delta STR}$*-GFP*, *Wsc1*$^{\Delta WSC}$*-GFP* and *Wsc1*$^{\Delta STR\Delta WSC}$*-GFP* cells were completely devoid of any clustering phenotype, with an enrichment at contacts close to ~2 (Figures 5D, 5E, and S2F–S2H). This indicates that the WSC and STR domains are required for protein clustering under force. However, given the long length of the rod-shape STR domains (estimated around 40–60 nm (Dupres et al., 2009; Kock et al., 2015)), one possible interpretation for the lack of *Wsc1*$^{\Delta STR}$*-GFP* clustering, is that the WSC domain is placed at a much lower "altitude" in the CW and cannot properly sense CW compression. To test this, we generated a Wsc1 allele in which the STR domain was swapped with that of the Mtl2 sensor, which does not form clusters. This swap construct exhibited a clustering phenotype similar to that of full-length Wsc1 (Figures 5D and 5E). We conclude that Wsc1 clustering under force is primarily driven by its extracellular WSC domain independently of cytoplasmic effectors.

Wsc1 clustering through restricted diffusivity in the membrane and CW

To understand mechanisms driving clustering under force, we next performed fluorescent recovery after photobleaching (FRAP) experiments. In cells growing in standard agar pads, Wsc1-GFP at free tips recovered with a half-time of ~188.7 ± 117 s (mean ± SD), ~1.2× higher than that of the integral membrane SNARE mCherry-Psy1 (Figures 6A and S6A–S6C) (Bendezú et al., 2015). FRAP images suggested that most of the recovery occurred along the membrane plane from lateral diffusive or advective transport (Figures S6B and S6C). Accordingly, FRAP half-times in an *end4Δ* mutant, defective in endocytosis, were nearly similar than in WT, suggesting that recycling does not contribute significantly to Wsc1 dynamics at these time scales (Figures S6A–S6C). Importantly, FRAP on clusters in microchannels revealed similar in-plane motility, but yielded a half-time significantly higher than at free tips: 457.3 ± 479 s (mean ± SD). In most clusters, we could observe some lateral recovery and diffusion. In a subset, Wsc1 appeared almost frozen, with no detectable recovery within the cluster, and half-times exceeding 15–20 min time scales. We note that these half-times, are ~two to three times faster than the typical timing for cluster formation seen in time lapses when cells grow and press onto each other (Figures 1C, 1E, and 1G). We propose that this difference may reflect the slower force-loading rate in these time lapses, limited by cell growth and rearrangements. Finally, *Wsc1*$^{\Delta WSC}$*-GFP* and *Wsc1*$^{\Delta STR}$*-GFP*, which are incapable of clustering, exhibited much smaller half-times—closer to that of mCherry-Psy1 (Figures 6A, 6B, and S6A).

To assess how CW mechanical compression may affect Wsc1 lateral diffusivity, we grew Wsc1-GFP and mCherry-Psy1 cells in channels and used the two-color assay to compute apposed CW thickness. We took a single midplane image in two colors to compute CW thickness and immediately performed FRAP in the GFP channel at the contact site. This revealed that Wsc1 recovered faster in CWs that were more relaxed as compared with those that were under high mechanical compression. Further, using a 2D diffusion model to estimate lateral diffusivity (Kang et al., 2012), we found that Wsc1 diffusivity decreased in dose dependence with CW mechanical compression (Figures 6C–6E). Together these results indicate that local mechanical stress on the CW may directly or indirectly hinder diffusion or reaction-diffusion of Wsc1 sensors within CWs, potentially contributing to their clustering behavior.

Functional relevance of Wsc1 clustering to CW integrity and cell survival

At free growing tips, Wsc1 co-localizes with downstream elements of the CWI: the Rho1 GEFs Rgf1 and Rgf2, the active form of Rho1, and the protein kinases Pck1 and Pck2 (García et al., 2006; Pérez et al., 2018) (Figure 7A). We co-imaged Wsc1-mCherry and Rgf1-GFP, Rgf2-GFP, Active Rho1-mECitrine, a marker for active GTP-bound Rho1, Pck1-GFP, and Pck2-GFP in cells bearing large compressive stress in channels. In multiple instances, we detected abnormal ectopic recruitment of these factors at cell sides, in close association with a Wsc1-mCherry cluster formed at lateral CW contact. Downstream cytoplasmic effectors were stable at these ectopic clusters for minutes, indicating that downstream transduction was taking place (Figures 7B, 7C, and S7A). We note, however, that the incidence of these lateral zones was relatively low (~10% to 20% of Wsc1 lateral clusters), and in most cells these downstream elements were recruited to growing tips. We interpret this as a result of a competition for CWI cytoplasmic effectors, with polar located ones that take over, given their association to tip-located polarity cues (Pérez et al., 2018). We conclude that Wsc1 clusters may serve as local "sensosome" platforms to recruit and activate downstream signaling elements to sites of mechanoperception.

To test the function of Wsc1 clusters in CW integrity more directly, we assayed cell survival. As Wsc1 is strictly required for survival in the absence of Mtl2 (Cruz et al., 2013), we used a shut-off construct for Mtl2, under the control of the low-expression *81xnmt1* promoter. In plates supplemented

Please cite this article in press as: Neeli-Venkata et al., Detection of surface forces by the cell-wall mechanosensor Wsc1 in yeast, Developmental Cell (2021), https://doi.org/10.1016/j.devcel.2021.09.024

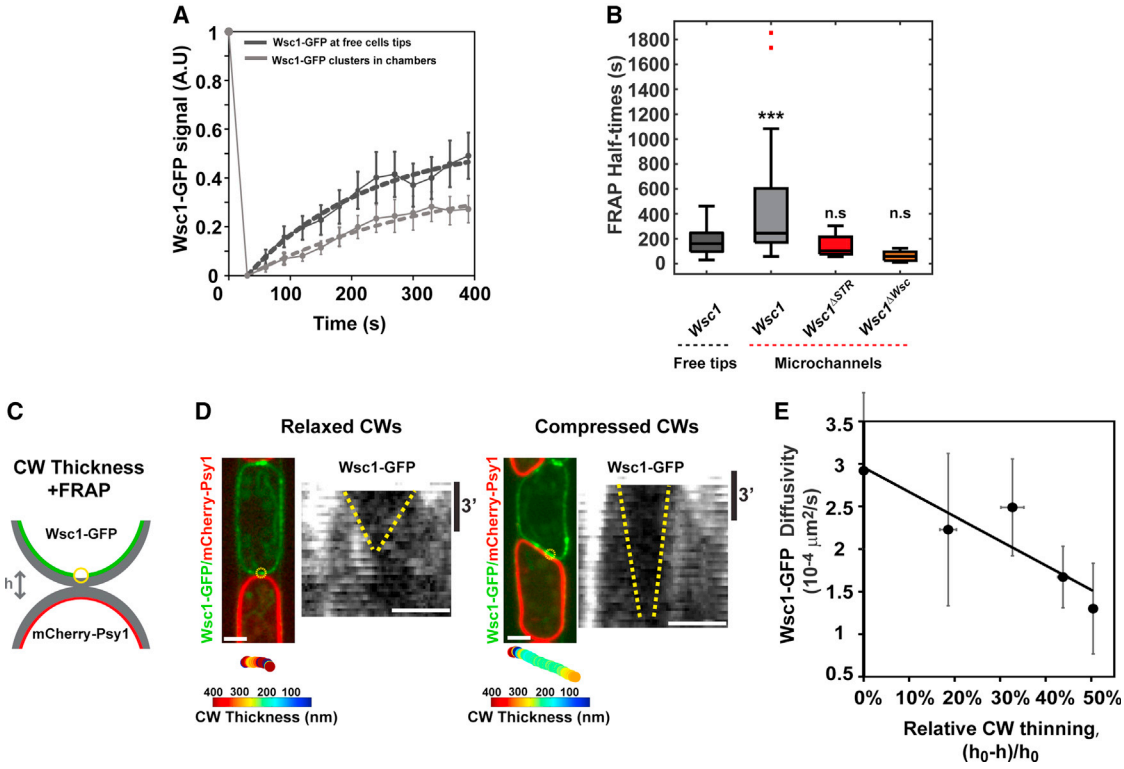

Figure 6. Cell wall compression hinders Wsc1 lateral diffusion

(A) Mean FRAP recovery curves of Wsc1-GFP at free tips or in clusters in microchannels (n = 28 and 27 cells, respectively, from 3 independent experiments). The dotted lines are exponential fits and error bars represent standard deviations.

(B) Box plots of FRAP half-times for the indicated conditions and alleles (n = 28, 27, 10, and 7 cells, respectively). Red dots are outliers in the distribution.

(C) Scheme representing the combination of a two-color assay as used in Figure 4C to compute CW thickness at contacts, combined with FRAP in the Wsc1-GFP expressing neighbor cell.

(D) Representative examples of relatively relaxed and compressed apposed CWs thickness at cell contacts, and Wsc1-GFP FRAP recovery dynamics represented with kymographs along a line scan around the contact area of 3 pixels in width. The yellow dotted lines mark signal recovery in the bleached area.

(E) Wsc1-GFP diffusivity estimated from FRAP data, plotted as a function of CW mechanical thinning. Each dot corresponds to a bin of 7 individual cells, and the line is a linear regression. Results were compared using a two-tailed non-parametric Mann-Whitney test. n.s. $p > 0.05$, ***, $p < 0.001$. Error bars are standard deviations. Scale bars, 2 μm.

with thiamine, to repress Mtl2 expression, *wsc1Δ*, *wsc1*$^{\Delta CC}$, *wsc1*$^{\Delta STR}$, and *wsc1*$^{\Delta STR\Delta WSC}$ were unable to grow. In contrast, *wsc1*$^{\Delta WSC}$ exhibited growth levels similar to wsc1 full length, suggesting that the WSC domain is dispensable for survival in the absence of Mtl2 in normal growth conditions (Figures S7D and S7E). This suggests that the *wsc1*$^{\Delta CC}$ is largely defective in downstream activation of the CWI, and that the STR "nanospring" domain is needed for survival in the absence of the other sensor in normal growth conditions.

In microchannels, where clusters form at high frequency, due to larger and more frequent compressive mechanical stresses onto the CWs, the survival behavior was markedly different. First, *wsc1Δ* cells exhibited a much higher yield of death of ~28%. Second, all alleles exhibited a high yield of death around ~25% including *wsc1*$^{\Delta WSC}$, which survives in normal growth conditions even in the absence of Mtl2. By imaging *wsc1*$^{\Delta CC}$-GFP, we could observe clusters that formed at a site of compression, followed by death of the two apposed cells, presumably because Wsc1, lacking its C-terminal tail, was unable to properly recruit and activate the CWI pathway to strengthen the CW subjected to large mechanical stress. Similar death events could also be recorded in *wsc1*$^{\Delta WSC}$-GFP cells, where downstream signaling is likely intact, but clusters cannot form (Figure S7B). To directly connect Wsc1 clustering and CW mechanical stress with death or survival, we grew *wsc1*$^{\Delta CC}$-GFP together with WT cells expressing mCherry-Psy1 and performed ~2-h time lapses to record lysis events and track Wsc1 clustering and CW thickness. In these videos, we did not detect any lysis in WT red cells, but a high incidence of dying *wsc1*$^{\Delta CC}$-GFP of ~26%. By analyzing dying or surviving cells at contact with a WT red cell, we found that lysing cells were preceded by a significantly higher Wsc1 enrichment, and thinner CWs, as compared with survivor cells (Figures 7E, 7F, and S7C). Together, these analyses suggest that Wsc1 clustering functions to detect local sites of CW mechanical compression and high stress to promote CW repair and survival.

DISCUSSION

Mechanosensation in the cell wall

The mechanics of the CW is largely recognized to support survival, morphogenesis, infection, and reproduction in organisms

Please cite this article in press as: Neeli-Venkata et al., Detection of surface forces by the cell-wall mechanosensor Wsc1 in yeast, Developmental Cell (2021), https://doi.org/10.1016/j.devcel.2021.09.024

CellPress

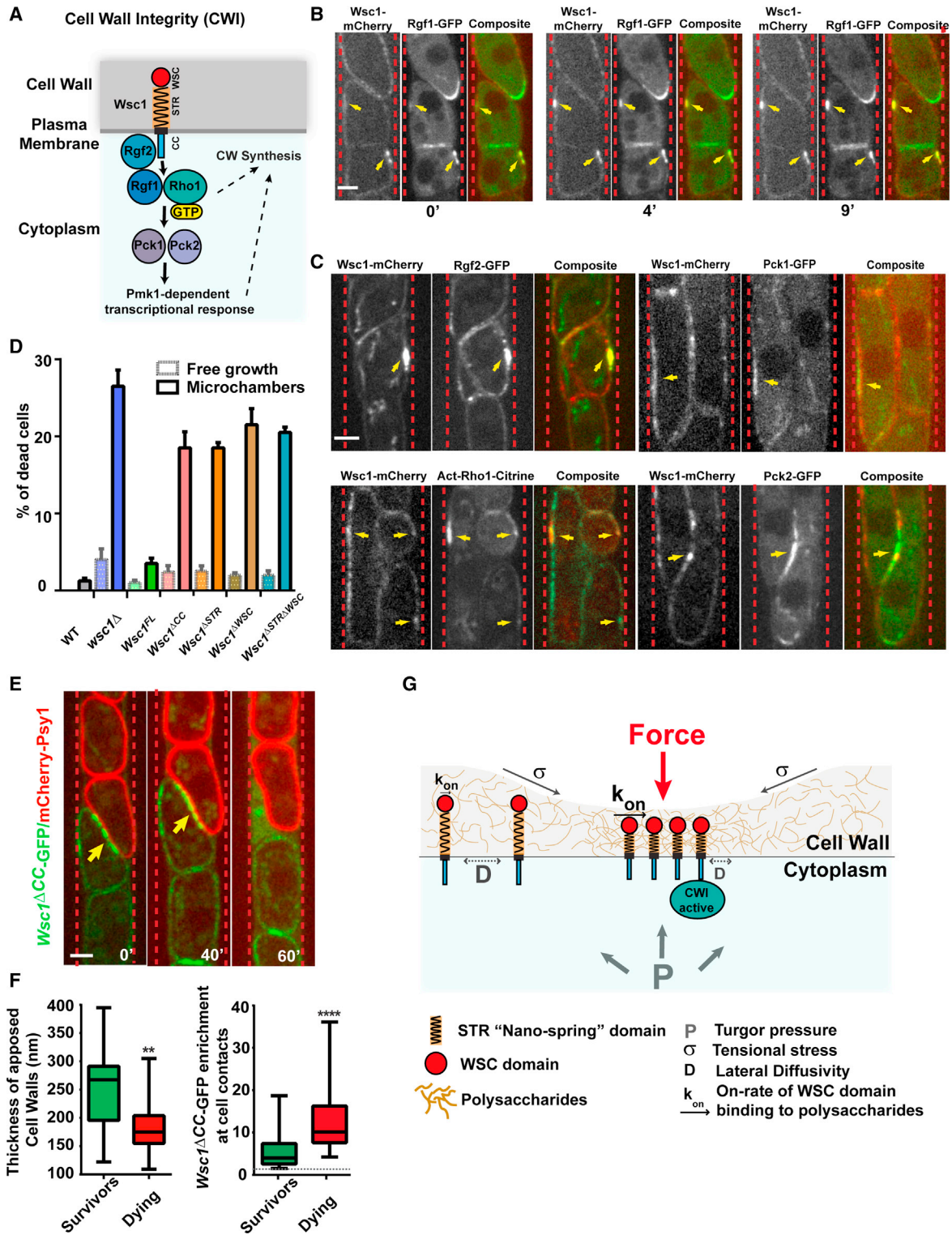

Figure 7. Force-dependent Wsc1 clusters recruit downstream signaling factors and promote cell survival

(A) Scheme representing Wsc1 and its domains in the membrane and CW and downstream cytoplasmic CWI components.

(B) Time lapse of cells grown in microchannels and co-expressing Wsc1-mCherry and Rgf1-GFP, showing the stable recruitment of downstream effectors to ectopic sites where Wsc1 clusters.

(C) Co-localization of Wsc1-mCherry with other downstream effectors of the CWI, featuring a clear visible ectopic accumulation at lateral sites where Wsc1-mCherry clusters (marked by yellow arrows).

(legend continued on next page)

Please cite this article in press as: Neeli-Venkata et al., Detection of surface forces by the cell-wall mechanosensor Wsc1 in yeast, Developmental Cell (2021), https://doi.org/10.1016/j.devcel.2021.09.024

ranging from bacteria to fungi and plants (Auer and Weibel, 2017; Banavar et al., 2018; Bastmeyer et al., 2002; Boudaoud, 2010; Davì and Minc, 2015; Ryder and Talbot, 2015; Wolf et al., 2012). To date, however, the bare notion of mechanosensation in the CW remains underappreciated and understudied. Progress has been limited in part by the lack of tractable readout of surface force sensing. By discovering that a conserved surface sensor embedded in the CW matrix can relocalize and accumulate at sites of mechanical compression on the CW, our study thus constitutes an important step in the emerging field of walled cell mechanobiology. Clusters formed in a range of conditions, spanning tip growth, septation, mating, and confinement, providing direct evidence, that even unicellular walled organisms can use surface mechanosensation to detect a contact with neighbors or obstacles. Importantly, our findings parallel with classical clustering phenotypes of mechanoreceptors, such as integrins and cadherins, under force, which have been pivotal to dissect mechanisms of mechanosensation in animal cells (Changede and Sheetz, 2017; Chen et al., 2017; Galbraith et al., 2002; Kechagia et al., 2019; Truong Quang et al., 2013). Thus, we anticipate that this work could open the route to studies on the mechanisms and functions of CW mechanosensation in yeast, fungi, and other walled cells.

Surface-sensor clustering

Seminal studies in *S. cerevisiae* had already reported on the formation of small Wsc1 foci/clusters, in normal growing cells, similar to what we observed here in *S. pombe* (Figure S1) (Heinisch et al., 2010; Kock et al., 2016). However, our observation that these clusters can grow to micrometric sizes and form at specific sites where the CW is compressed places Wsc1 as a *bona fide* mechanosensor, and raises the important question of how it may sense force. Our genetic analysis suggests that clustering under force does not implicate canonical regulators of membrane trafficking, polarity and CWI. In addition, while removal of the Wsc1 cytoplasmic C-terminal domain did not affect clustering, removal of any of the CW-associated extracellular domains completely abolishes it. Also, swapping the STR domain with that of the nonclustering Mtl2 suggested that the WSC domain is the main extracellular domain to promote clustering. These data strongly support that most of the ability to sense and accumulate in response to forces is encoded in the extracellular Wsc1 domains, placing Wsc1 as a potential autonomous sensor of surface forces.

One previously proposed mechanism for Wsc1 clustering in *S. cerevisiae*, is that the high content of cysteine residues in the WSC domain may favor protein-protein *cis* interactions through disulfide bond formation (Kock et al., 2016). However, our observation that clusters can disassemble within a few minutes when CWs are relaxed does not simply align with the role of covalent interactions. Rather, our FRAP data and allele analysis supports a model based on restricted local diffusivity, and weak interactions between the WSC domain and CW polysaccharides. In that view, we posit that local CW compression, and/or consequent tensile lateral stress could modulate the density/arrangement of the CW matrix favoring the binding of WSC domains to polysaccharides, thereby reducing lateral diffusivity and promoting clustering (Figure 7G). In addition, as the STR "nanospring" domain mediates downstream transduction, we propose that its natural conformation is stretched and that it compresses along with the CW, when force is applied, presumably driving conformational changes and/or phosphorylation of the cytoplasmic C-terminal domain for CWI activation (Figure 7G). Accordingly, AFM-based measurement of the stiffness of the STR suggests that it is two to three orders of magnitude softer than the CW, so that its length should directly follow the position of the WSC domain above that moves transversally in response to CW compression. Our proposed model has conceptual equivalence to "kinetic trap" models for integrin clustering, in which integrin interactions with ECM ligands reduces lateral diffusivity and promote clustering (Ballestrem et al., 2001; Kechagia et al., 2019; Laukaitis et al., 2001; Paszek et al., 2009; Welf et al., 2012). Importantly, our model could presumably allow Wsc1 to detect multiple CW parameters, including thickness, elasticity, stress, or strain, which cannot be easily disentangled in our experiments. Finer molecular dissection, local manipulation of CW matrices, as well as more resolved methods to control force application onto the surface, may help to refine and expand these initial CW mechanosensing models.

Implication for cell physiology and survival

Clustering is a conserved feature of sensors to form "sensosome" platforms, which serve as hubs for signal perception and transmission. Accordingly, our data suggest that Wsc1 clusters can recruit downstream CWI elements and promote survival under large and more frequent stresses encountered in microchannels. We could not assay transcriptional activation given that *S. pombe* Pmk1 localizes to both cytoplasm and nucleus independently of stress-induced activation of the pathway (Madrid et al., 2006). The physiological relevance of microchannels to natural yeast or fungal habitat may include dense colonies or biofilms. In addition, we provide significant evidence that clusters form even in classical dilute growth assays, albeit more transiently, at sites of cell-cell contacts when cells grow and collide onto each other at the end of septation, or at growing tips in interphase. We also observed smaller dynamic clusters at free

(D) Quantification of cell death in different Wsc1 alleles, in agar pad (free growth) or in packed microchannels (n ~ 600 cells for each allele, from 2 independent experiments).

(E) Time lapse of *Wsc1$^{\Delta CC}$-GFP* cells growing against WT cells expressing mCherry-psy1, which compress CWs, form clusters, and undergo cell lysis.

(F) (Left) Quantification of apposed CW thickness at contacts between WT cells expressing mCherry-psy1 and surviving or dying cells expressing *Wsc1$^{\Delta CC}$-GFP* (n= 14 and 16 cells). (Right) Quantification of *Wsc1$^{\Delta CC}$-GFP* enrichment in surviving or dying cells at a contact with a WT cell expressing mCherry-psy1 (n = 108 and 66 cells).

(G) Proposed model for Wsc1 mechanosensation. Wsc1 diffuses in the membrane and CW planes and interacts with CW polysaccharides through its WSC domain. Upon force application, the CW is locally compressed, promoting the densification/rearrangement of CW sugars, which enhances the binding kinetics of WSC domains to sugars, slowing down lateral diffusivity, and leading to cluster formation. In parallel, the STR domain becomes compressed to trigger downstream CWI activation through the cytoplasmic C-terminal domain. Results were compared by using a two-tailed non-parametric Mann-Whitney test. n.s. **p < 0.01; ****p < 0.0001. Error bars are standard deviations. Scale bars, 2 μm.

growing tips independently of any contact. Although we have not yet explored the significance of these clusters, we suspect that they could correspond to local sites of CW thinning or higher stress (Figure S1A). Wsc1-mediated mechanosensation could thus represent a basal homeostatic module contributing to homogenize CW mechanics at remodeling growth sites (Banavar et al., 2018; Davì et al., 2018). Finally, we also observe massive clustering at sites of mating-tip contacts. MID-type sensors were first identified from the analysis of "mating induced death" mutants in *S. cerevisiae* (Ono et al., 1994), and functions of WSC-types sensors have also been recently suggested for mating in these cells (Banavar et al., 2018). The accumulation of Wsc1 at mating-tip contacts suggests that it could act to slow down or buffer CW digestion. Future studies incorporating the notion of CW mechanosensation in the regulation of growth, reproduction, survival, or microbial infection promise to highlight the role of mechanical feedbacks in the basic lifestyles of walled cells.

Limitations of the study

Although our study establishes Wsc1 as a local mechanosensor for the CW, it relies on indirect modulations and estimations of surface stress. As such, for instance, we cannot presently discern whether Wsc1 senses a given threshold in surface force or a force-loading rate or a more subtle combination of both. Similarly, we use CW thickness as a proxy for mechanical compression, but whether Wsc1 directly senses thickness, tension, or stress remains to be tested. Finally, we provide evidence that Wsc1 clusters serve to promote the activation of the CWI pathway, which presumably reinforces the CW to limit surface stress. However, our data are limited to: (1) viability studies in situations of high surface stress and in multiple Wsc1 truncated alleles and (2) the observation of the stable recruitment of several downstream effectors of the CWI at sites where Wsc1 clusters. Whether these clusters act as real "sensosomes," and which components they may recruit, remain to be further studied by biochemical interaction studies.

STAR★METHODS

Detailed methods are provided in the online version of this paper and include the following:

- KEY RESOURCES TABLE
- RESOURCE AVAILABILITY
  - Lead contact
  - Materials availability
  - Data and code availability
- EXPERIMENTAL MODEL AND SUBJECT DETAILS
  - Fission yeast strains and growth conditions
- METHOD DETAILS
  - Cloning and yeast genetics
  - Mating assays
  - Micro-fabricated channels and microwells handling
  - Pharmacological inhibition
  - Turgor pressure manipulation using various sorbitol doses
  - Cell death assays
  - Microscopy
- QUANTIFICATION AND STATISTICAL ANALYSIS
  - Image analysis and quantifications
  - Statistical Analysis

SUPPLEMENTAL INFORMATION

Supplemental information can be found online at https://doi.org/10.1016/j.devcel.2021.09.024.

ACKNOWLEDGMENTS

We thank S.Martin, P. Perez, and K. Gould's labs for sharing strains and reagents, as well as our colleagues A. Boudaoud and S. Lon for carefully reading this manuscript. We gratefully thank all members of the Minc and Sanchez teams, and V. Albanese for discussion and technical help. This work was supported by the MEIC, Spain (BFU2017-84508-P) and the Regional Government of Castile and Leon [SA073U14] to Y.S., and the Centre National de la Recherche Scientifique (CNRS), the Agence Nationale pour la Recherche ("Cell size" no. ANR-14-CE11-0009-02 and "CellWallSense" no. ANR-20-CE13-0003-01), La Ligue Contre le Cancer (EL2021.LNCC/ NiM), and the European Research Council (ERC CoG "Forcaster" no. 647073) to N.M.

AUTHOR CONTRIBUTIONS

Conceptualization, N.M., Y.S., and R.N.V.; methodology, N.M., Y.S., R.C., C.M.D., and R.N.V.; Original draft, N.M., C.M.D., and R.N.V.; draft editing, N.M., Y.S., C.M.D., and R.N.V.

DECLARATION OF INTERESTS

The authors declare no competing interests.

Received: December 4, 2020
Revised: July 13, 2021
Accepted: September 24, 2021
Published: October 18, 2021

REFERENCES

Abenza, J.F., Couturier, E., Dodgson, J., Dickmann, J., Chessel, A., Dumais, J., and Salas, R.E.C. (2015). Wall mechanics and exocytosis define the shape of growth domains in fission yeast. Nat. Commun. *6*, 8400.

Atilgan, E., Magidson, V., Khodjakov, A., and Chang, F. (2015). Morphogenesis of the fission yeast cell through cell wall expansion. Curr. Biol. *25*, 2150–2157.

Auer, G.K., and Weibel, D.B. (2017). Bacterial cell mechanics. Biochemistry *56*, 3710–3724.

Bähler, J., Wu, J.Q., Longtine, M.S., Shah, N.G., McKenzie, A., 3rd, Steever, A.B., Wach, A., Philippsen, P., and Pringle, J.R. (1998). Heterologous modules for efficient and versatile PCR-based gene targeting in Schizosaccharomyces pombe. Yeast *14*, 943–951.

Ballestrem, C., Hinz, B., Imhof, B.A., and Wehrle-Haller, B. (2001). Marching at the front and dragging behind: differential alphaVbeta3-integrin turnover regulates focal adhesion behavior. J. Cell Biol. *155*, 1319–1332.

Banavar, S.P., Gomez, C., Trogdon, M., Petzold, L.R., Yi, T.M., and Campàs, O. (2018). Mechanical feedback coordinates cell wall expansion and assembly in yeast mating morphogenesis. PLoS Comput. Biol. *14*, e1005940.

Bastmeyer, M., Deising, H.B., and Bechinger, C. (2002). Force exertion in fungal infection. Annu. Rev. Biophys. Biomol. Struct. *31*, 321–341.

Bendezú, F.O., Vincenzetti, V., Vavylonis, D., Wyss, R., Vogel, H., and Martin, S.G. (2015). Spontaneous Cdc42 polarization independent of GDI-mediated extraction and actin-based trafficking. PLoS Biol. *13*, e1002097.

Bonazzi, D., Julien, J.D., Romao, M., Seddiki, R., Piel, M., Boudaoud, A., and Minc, N. (2014). Symmetry breaking in spore germination relies on an interplay between polar cap stability and spore wall mechanics. Dev. Cell *28*, 534–546.

Boudaoud, A. (2010). An introduction to the mechanics of morphogenesis for plant biologists. Trends Plant Sci. *15*, 353–360.

Changede, R., and Sheetz, M. (2017). Integrin and cadherin clusters: a robust way to organize adhesions for cell mechanics. BioEssays *39*, 1–12.

Chen, Y., Ju, L., Rushdi, M., Ge, C., and Zhu, C. (2017). Receptor-mediated cell mechanosensing. Mol. Biol. Cell *28*, 3134–3155.

Colin, L., Chevallier, A., Tsugawa, S., Gacon, F., Godin, C., Viasnoff, V., Saunders, T.E., and Hamant, O. (2020). Cortical tension overrides geometrical cues to orient microtubules in confined protoplasts. Proc. Natl. Acad. Sci. USA *117*, 32731–32738.

Cruz, S., Muñoz, S., Manjón, E., García, P., and Sanchez, Y. (2013). The fission yeast cell wall stress sensor-like proteins Mtl2 and Wsc1 act by turning on the GTPase Rho1p but act independently of the cell wall integrity pathway. MicrobiologyOpen *2*, 778–794.

Davì, V., Chevalier, L., Guo, H., Tanimoto, H., Barrett, K., Couturier, E., Boudaoud, A., and Minc, N. (2019). Systematic mapping of cell wall mechanics in the regulation of cell morphogenesis. Proc. Natl. Acad. Sci. USA *116*, 13833–13838.

Davì, V., and Minc, N. (2015). Mechanics and morphogenesis of fission yeast cells. Curr. Opin. Microbiol. *28*, 36–45.

Davì, V., Tanimoto, H., Ershov, D., Haupt, A., De Belly, H., Le Borgne, R., Couturier, E., Boudaoud, A., and Minc, N. (2018). Mechanosensation dynamically coordinates polar growth and cell wall assembly to promote cell survival. Dev. Cell *45*, 170–182.e7.

Dudin, O., Bendezú, F.O., Groux, R., Laroche, T., Seitz, A., and Martin, S.G. (2015). A formin-nucleated actin aster concentrates cell wall hydrolases for cell fusion in fission yeast. J. Cell Biol. *208*, 897–911.

Dupres, V., Alsteens, D., Wilk, S., Hansen, B., Heinisch, J.J., and Dufrêne, Y.F. (2009). The yeast Wsc1 cell surface sensor behaves like a nanospring in vivo. Nat. Chem. Biol. *5*, 857–862.

Elhasi, T., and Blomberg, A. (2019). Integrins in disguise - mechanosensors in Saccharomyces cerevisiae as functional integrin analogues. Microb. Cell *6*, 335–355.

Forsburg, S.L., and Rhind, N. (2006). Basic methods for fission yeast. Yeast *23*, 173–183.

Galbraith, C.G., Yamada, K.M., and Sheetz, M.P. (2002). The relationship between force and focal complex development. J. Cell Biol. *159*, 695–705.

García, P., Tajadura, V., García, I., and Sánchez, Y. (2006). Rgf1p is a specific Rho1-GEF that coordinates cell polarization with cell wall biogenesis in fission yeast. Mol. Biol. Cell *17*, 1620–1631.

Hamann, T., and Denness, L. (2011). Cell wall integrity maintenance in plants: lessons to be learned from yeast? Plant Signal. Behav. *6*, 1706–1709.

Hartman, N.C., and Groves, J.T. (2011). Signaling clusters in the cell membrane. Curr. Opin. Cell Biol. *23*, 370–376.

Haupt, A., Ershov, D., and Minc, N. (2018). A positive feedback between growth and polarity provides directional persistency and flexibility to the process of tip growth. Curr. Biol. *28*, 3342–3351.e3.

Heinisch, J.J., Dupres, V., Wilk, S., Jendretzki, A., and Dufrêne, Y.F. (2010). Single-molecule atomic force microscopy reveals clustering of the yeast plasma-membrane sensor Wsc1. PLoS One *5*, e11104.

Imai, Y., Miyake, S., Hughes, D.A., and Yamamoto, M. (1991). Identification of a GTPase-activating protein homolog in Schizosaccharomyces pombe. Mol. Cell. Biol. *11*, 3088–3094.

Kang, M., Day, C.A., Kenworthy, A.K., and DiBenedetto, E. (2012). Simplified equation to extract diffusion coefficients from confocal FRAP data. Traffic *13*, 1589–1600.

Kechagia, J.Z., Ivaska, J., and Roca-Cusachs, P. (2019). Integrins as biomechanical sensors of the microenvironment. Nat. Rev. Mol. Cell Biol. *20*, 457–473.

Kock, C., Arlt, H., Ungermann, C., and Heinisch, J.J. (2016). Yeast cell wall integrity sensors form specific plasma membrane microdomains important for signalling. Cell. Microbiol. *18*, 1251–1267.

Kock, C., Dufrêne, Y.F., and Heinisch, J.J. (2015). Up against the wall: is yeast cell wall integrity ensured by mechanosensing in plasma membrane microdomains? Appl. Environ. Microbiol. *81*, 806–811.

Ladoux, B., and Mège, R.M. (2017). Mechanobiology of collective cell behaviours. Nat. Rev. Mol. Cell Biol. *18*, 743–757.

Laukaitis, C.M., Webb, D.J., Donais, K., and Horwitz, A.F. (2001). Differential dynamics of alpha 5 integrin, paxillin, and alpha-actinin during formation and disassembly of adhesions in migrating cells. J. Cell Biol. *153*, 1427–1440.

Levin, D.E. (2011). Regulation of cell wall biogenesis in Saccharomyces cerevisiae: the cell wall integrity signaling pathway. Genetics *189*, 1145–1175.

Madrid, M., Soto, T., Khong, H.K., Franco, A., Vicente, J., Pérez, P., Gacto, M., and Cansado, J. (2006). Stress-induced response, localization, and regulation of the Pmk1 cell integrity pathway in Schizosaccharomyces pombe. J. Biol. Chem. *281*, 2033–2043.

Martin, S.G., and Arkowitz, R.A. (2014). Cell polarization in budding and fission yeasts. FEMS Microbiol. Rev. *38*, 228–253.

Merlini, L., Khalili, B., Dudin, O., Michon, L., Vincenzetti, V., and Martin, S.G. (2018). Inhibition of Ras activity coordinates cell fusion with cell-cell contact during yeast mating. J. Cell Biol. *217*, 1467–1483.

Minc, N., Boudaoud, A., and Chang, F. (2009a). Mechanical forces of fission yeast growth. Curr. Biol. *19*, 1096–1101.

Minc, N., Bratman, S.V., Basu, R., and Chang, F. (2009b). Establishing new sites of polarization by microtubules. Curr. Biol. *19*, 83–94.

Mishra, R., van Drogen, F., Dechant, R., Oh, S., Jeon, N.L., Lee, S.S., and Peter, M. (2017). Protein kinase C and calcineurin cooperatively mediate cell survival under compressive mechanical stress. Proc. Natl. Acad. Sci. USA *114*, 13471–13476.

Moreno, S., Klar, A., and Nurse, P. (1991). Molecular genetic analysis of fission yeast Schizosaccharomyces pombe. Methods Enzymol. *194*, 795–823.

Moreno-Layseca, P., Icha, J., Hamidi, H., and Ivaska, J. (2019). Integrin trafficking in cells and tissues. Nat. Cell Biol. *21*, 122–132.

Ohmiya, R., Yamada, H., Nakashima, K., Aiba, H., and Mizuno, T. (1995). Osmoregulation of fission yeast: cloning of two distinct genes encoding glycerol-3-phosphate dehydrogenase, one of which is responsible for osmotolerance for growth. Mol. Microbiol. *18*, 963–973.

Ono, T., Suzuki, T., Anraku, Y., and Iida, H. (1994). The MID2 gene encodes a putative integral membrane protein with a Ca(2+)-binding domain and shows mating pheromone-stimulated expression in Saccharomyces cerevisiae. Gene *151*, 203–208.

Paszek, M.J., Boettiger, D., Weaver, V.M., and Hammer, D.A. (2009). Integrin clustering is driven by mechanical resistance from the glycocalyx and the substrate. PLoS Comput. Biol. *5*, e1000604.

Pérez, P., Cortés, J.C.G., Cansado, J., and Ribas, J.C. (2018). Fission yeast cell wall biosynthesis and cell integrity signalling. Cell Surf. *4*, 1–9.

Philip, B., and Levin, D.E. (2001). Wsc1 and Mid2 are cell surface sensors for cell wall integrity signaling that act through Rom2, a guanine nucleotide exchange factor for Rho1. Mol. Cell. Biol. *21*, 271–280.

Ryder, L.S., and Talbot, N.J. (2015). Regulation of appressorium development in pathogenic fungi. Curr. Opin. Plant Biol. *26*, 8–13.

Sato, M., Dhut, S., and Toda, T. (2005). New drug-resistant cassettes for gene disruption and epitope tagging in Schizosaccharomyces pombe. Yeast *22*, 583–591.

Snaith, H.A., Samejima, I., and Sawin, K.E. (2005). Multistep and multimode cortical anchoring of tea1p at cell tips in fission yeast. EMBO J. *24*, 3690–3699.

Truong Quang, B.A., Mani, M., Markova, O., Lecuit, T., and Lenne, P.F. (2013). Principles of E-cadherin supramolecular organization in vivo. Curr. Biol. *23*, 2197–2207.

Vještica, A., Marek, M., Nkosi, P.J., Merlini, L., Liu, G., Bérard, M., Billault-Chaumartin, I., and Martin, S.G. (2020). A toolbox of stable integration vectors in the fission yeast Schizosaccharomyces pombe. J. Cell Sci. *133*, jcs240754.

Vjestica, A., Merlini, L., Dudin, O., Bendezu, F.O., and Martin, S.G. (2016). Microscopy of fission yeast sexual lifecycle. J. Vis. Exp. *109*, 53801.

Vogel, V., and Sheetz, M. (2006). Local force and geometry sensing regulate cell functions. Nat. Rev. Mol. Cell Biol. *7*, 265–275.

Vu, M.H., Iswanto, A.B.B., Lee, J., and Kim, J.-Y. (2020). The role of plasmodesmata-associated receptor in plant development and environmental response. Plants (Basel) *9*, 216.

Wawra, S., Fesel, P., Widmer, H., Neumann, U., Lahrmann, U., Becker, S., Hehemann, J.H., Langen, G., and Zuccaro, A. (2019). FGB1 and WSC3 are in planta-induced beta-glucan-binding fungal lectins with different functions. New Phytol. *222*, 1493–1506.

Welf, E.S., Naik, U.P., and Ogunnaike, B.A. (2012). A spatial model for integrin clustering as a result of feedback between integrin activation and integrin binding. Biophys. J. *103*, 1379–1389.

Wolf, S., Hématy, K., and Höfte, H. (2012). Growth control and cell wall signaling in plants. Annu. Rev. Plant Biol. *63*, 381–407.

Zegman, Y., Bonazzi, D., and Minc, N. (2015). Measurement and manipulation of cell size parameters in fission yeast. Methods Cell Biol. *125*, 423–436.

Please cite this article in press as: Neeli-Venkata et al., Detection of surface forces by the cell-wall mechanosensor Wsc1 in yeast, Developmental Cell (2021), https://doi.org/10.1016/j.devcel.2021.09.024

STAR★METHODS

KEY RESOURCES TABLE

REAGENT or RESOURCE	SOURCE	IDENTIFIER
Experimental Models: Organisms/ Strains		
h⁻ leu1-32 ura4D-18	Sanchez lab stocks	SM215
h⁻ wsc1-GFP:ura4⁺ leu1-32 ade6M210 ura4D-18 his3DI	Sanchez lab stocks	GRG45
h⁻ wsc1::ura⁺ leu1-32 ade6M210 ura4D-18 his3DI	Sanchez lab stocks	GRG8
h⁻ wsc1::his3⁺ leu1-32 ade6M210 ura4D-18 his3DI	Sanchez lab stocks	SC136
h⁻ wsc1::kan⁺ leu1-32 ade6M210 ura4D-18 his3DI	Sanchez lab stocks	GRG15
h⁻ mtl2::his3 ura4d18 leu1-32 ade6M210 his3DI	Sanchez lab stocks	YS1220
h⁻ kan-81xnmt1-mtl2⁺ leu1-32 ura4D18 his3D ade6M210	Sanchez lab stocks	SC33
h⁻ mtl2::kan ura4d18 leu1-32 ade6M210 his3DI	Sanchez lab stocks	SC92
h⁺ kan-P81xnmt1-mtl2⁺ wsc1::ura⁺ leu1-32 ura4D18 his3D ade6M210	Sanchez lab stocks	SC80
h⁻ wsc1-GFP:ura4⁺ mtl2::kan his3D1 leu1-32 ade6M210	Sanchez lab stocks	SC255
h90 leu1-32 ade6M210 ura4D-18	Minc lab stocks	DB146
h+ wsc1-GFP:ura4+ leu1-32 ade6M210 ura4D-18	Minc lab stocks	RN19
h- wsc1-GFP:ura4+ leu1-32 ade6M210 ura4D-18	Minc lab stocks	RN73
h- mtl2-GFP:ura4+ leu1-32 ade6M210 ura4D-18	Minc lab stocks	RN21
h+ leu:mCherry-psy1 ura4-D18 ade-	Minc lab stocks	NM448
h90 leu:mCherry-psy1 ura4-D18 ade-	Minc lab stocks	NM447
h90 wsc1-GFP:ura4+ leu1-32 ura4D-18 ade-	This paper	RN42
h+ wsc1-mCherry:KanMX leu1-32 ade6M210 ura4D-18	This paper	RN48
h90 wsc1:: KanMX leu1-32 ade6M210 ura4D-18	This paper	RN51
h90 wsc1-GFP:ura4+ leu:mCherry-Psy1 ura4D-18 ade-	This paper	RN46
h90 wsc1-mCherry:KanMX mtl2-GFP:ura4+	This paper	RN57
h- wsc1-GFP:ura4+ cdc25-22	This paper	RN58
h90 wsc1-GFP:ura4+gap1::hphMX	This paper	RN126
h90 wsc1-GFP:ura4+fus1:: KanMX	This paper	RN127
h90 wsc1-GFP:ura4+ ade6+:ptdh1:3mTagBFP2-Ritc:terminatorScADH1:bsdMX	This paper	RN170
h90 wsc1-mCherry:KanMX CRIB-3GFP:ura leu1-32 ura4-D18	This paper	RN54
h90 wsc1-GFP:ura4+ bgs4::ura4 RFP-bgs4-Leu ade-	This paper	RN91
h90 wsc1-GFP:ura4+ mCherry-atb2:hphMX	This paper	RN253
h90 wsc1-GFP:ura4+ tea4::KanMX	This paper	RN251
h90 wsc1-GFP:ura4+ tea1::NatMX	This paper	RN255
h90 wsc1-GFP:ura4+ pom1::NatMX	This paper	RN256
h90 wsc1-GFP:ura4+ end4::KanMX leu1-32 ura4-D18 ade-	This paper	RN82
h90 wsc1-GFP:ura4 wsp1::leu ade-	This paper	RN90
h90 wsc1-GFP:ura4+ myo1::KanMX	This paper	RN186
h90 wsc1-GFP:ura4+ exo70::KanMX leu1-32 ura4-D18 ade-	This paper	RN88
h90 wsc1-GFP:ura4+ sec8-1 ade6 Leu1-32 ura4-D18	This paper	RN152

(*Continued on next page*)

Please cite this article in press as: Neeli-Venkata et al., Detection of surface forces by the cell-wall mechanosensor Wsc1 in yeast, Developmental Cell (2021), https://doi.org/10.1016/j.devcel.2021.09.024

Continued

REAGENT or RESOURCE	SOURCE	IDENTIFIER
h90 wsc1-GFP:ura4+ mal3::NatMX	This paper	RN266
h90 wsc1-GFP:ura4+ for3::KanMX	This paper	RN84
h90 wsc1-GFP:ura4+ myo52::KanMX	This paper	RN138
h90 wsc1-GFP:ura4+ orb6-25 ade6-M210 leu1-32	This paper	RN107
h90 wsc1-GFP:ura4+ cwg 1-1	This paper	RN153
h90 wsc1-GFP:ura4+spn1::KanMX	This paper	RN264
h90 wsc1-GFP:ura4+spn4::KanMX	This paper	RN265
h90 wsc1-GFP:ura4+ pck1::KanMX leu1-32 ura4-D18ade-	This paper	RN77
h90 wsc1-GFP:ura4+ pmk1::KanMX leu1-32 ura4-D18 ade-	This paper	RN76
h90 wsc1-GFP:ura4+ sty1::kanMX leu1-32 ura4-D18 ade-	This paper	RN143
h90 wsc1-GFP:ura4+ rgf1::KanMX leu1-32 ura4-D18 ade-	This paper	RN109
h90 wsc1-GFP:ura4+ rgf2::KanMX leu1-32 ura4-D18 ade-	This paper	RN86
h90 wsc1-GFP:ura4+ mtl2::KanMX leu1-32 ura4-D18 ade-	This paper	RN129
h90 wsc1-GFP:ura4+ gpd1::NatMX	This paper	RN250
h90 wsc1-GFP:ura4+ msy2::KanMX	This paper	RN267
h⁻ wsc1 $^{\Delta WSC}$ -GFP:ura4⁺ leu1-32 ade6M210 ura4D-18 his3DI	This paper	RC90
h⁻ wsc1$^{\Delta STR}$-GFP:ura4⁺ leu1-32 ade6M210 ura4D-18 his3DI	This paper	RC96
h⁻ wsc1$^{\Delta STR\Delta WSC}$-GFP:ura4⁺ leu1-32 ade6M210 ura4D-18 his3DI	This paper	RC98
h⁻ wsc1 $^{\Delta CC}$-GFP:ura4⁺ leu1-32 ade6M210 ura4D-18 his3DI	This paper	RC91
h90 wsc1 $^{\Delta CC}$-GFP:ura4⁺ leu1-32 ade6M210 ura4D-18	This paper	RN116
h90 wsc1$^{\Delta STR}$-GFP:ura4⁺ leu1-32 ade6M210 ura4D-18	This paper	RN122
h90 wsc1 $^{\Delta WSC}$ -GFP:ura4⁺ leu1-32 ade6M210 ura4D-18	This paper	RN112
h90 wsc1$^{\Delta STR\Delta WSC}$-GFP:ura4⁺ leu1-32 ade6M210 ura4D-18	This paper	RN125
h90 wsc1-mCherry:KanMX leu1:rgf1-GFP	This paper	RN62
h90 wsc1-mCherry:NatMX + Plasmid pAL-rgf2⁺-8ala-GFP	This paper	RN268
h90 wsc1-mCherry:NatMX leu1::KanMX-P3nmt1-pkc1(HR1-C2)-mECitrine	This paper	RN63
h90 wsc1-mCherry:NatMX pck1::pck1-GFP-HA-KanMX	This paper	RN145
h90 wsc1-mCherry:NatMX pck2::pck2-GFP-HA-KanMX	This paper	RN146
h90 wsc1^{FL}:ura4+ leu1-32 ade6M210 ura4D-18	This paper	RN176
h90 wsc1 $^{\Delta CC}$:ura4+ leu1-32 ade6M210 ura4D-18	This paper	RN178
h90 wsc1$^{\Delta STR}$:ura4+ leu1-32 ade6M210 ura4D-18	This paper	RN182
h90 wsc1 $^{\Delta WSC}$:ura4+ leu1-32 ade6M210 ura4D-18	This paper	RN180
h90 wsc1$^{\Delta STR\Delta WSC}$:ura4+ leu1-32 ade6M210 ura4D-18	This paper	RN184
h90 wsc1$^{\Delta STR\ MTL2\text{-}STR}$-GFP:ura4⁺ leu1-32 ura4D-18	This paper	RN222
h90 mtl2-GFP:ura4+ leu1-32 ade6M210 ura4D-18	This paper	RN43

(*Continued on next page*)

Please cite this article in press as: Neeli-Venkata et al., Detection of surface forces by the cell-wall mechanosensor Wsc1 in yeast, Developmental Cell (2021), https://doi.org/10.1016/j.devcel.2021.09.024

Continued

REAGENT or RESOURCE	SOURCE	IDENTIFIER
h⁺ wsc1 $^{\Delta WSC}$:ura4⁺ kan-P81xnmt1-mtl2⁺ leu1-32 ura4D18 ade6M210	This paper	YS5505
h⁺ wsc1 $^{\Delta WSC\ \Delta STR}$:ura4⁺ kan-P81xnmt1-mtl2⁺ leu1-32 ura4D18 ade6M210	This paper	YS5485
h⁺ wsc1 $^{\Delta CC}$:ura4⁺ kan-P81xnmt1-mtl2⁺ leu1-32 ura4D18 ade6M210	This paper	YS5504
h⁻ wsc1$^{\Delta STR\ MTL2\text{-}STR}$-GFP:ura4⁺ leu1-32 ade6M210 ura4D-18	This paper	YS5509
h⁻ wsc1$^{\Delta TMD}$-GFP:ura4⁺ leu1-32 ade6M210 ura4D-18	This paper	YS5595
Chemicals		
Glusulase	PerkinElmer	Cat# NEE154001EA
Methyl 2-Benzimidazole Carbamate (Carbendazim, MBC)	Sigma-Aldrich	Cat# 378674
Pluronic acid	Sigma-Aldrich	Cat# P2443
D-Sorbitol	Sigma-Aldrich	Cat# S1876
Caspofungin	Sigma-Aldrich	Cat# SML0425
Dimethyl Sulphoxide (DMSO)	Euromedex	Cat# SC-358801
Percoll	Sigma-Aldrich	Cat# P1644
PDMS kit (Sylgard 184)	Dow Corning	Cat# DC184
Oligonucleotides		
wsc1-mCherry 5'forward (*wsc1* homology underlined):TGATGAATCGCAAATCAAG TGAATCTTTGGCTGACAGTCAGGATTA TTCGAGAAAGATATTGCGTGTCACAAA TTTGAACCGGATCCCCGGGTTAATTAA	This paper	RN01
wsc1-mCherry 5'reverse (*wsc1* homology underlined):ATTATGAAAGTCATAAACAC CATAAAGAAGAAATAATTTTTTGGTTGAA TTTAAATAAAGTAAAAAAGAAAAATGTTG TTGAATTCGAGCTCGTTTAAAC	This paper	RN02
Resistance marker switching 5'forward: CGGATCCCCGGGTTAATTAAGGCG	(Sato et al., 2005)	MD1
Resistance marker switching 5'reverse: GAATTCGAGCTCGTTTAAACACTGGAT GGCGGCGTTAGTATCG	(Sato et al., 2005)	MD2
wsc1$^{\Delta WSC}$ primer 5'forward to eliminate from +93 bp to +351 bp: GGTTTGCAAAACCCCATTGCCAGTAG CGCTCATGTCAGCCGCCACCAACCGAGT	This paper	N/A
wsc1$^{\Delta STR}$ primer 5'forward to eliminate from +354 bp to +846 bp: GCATTCAAGGACGTATGGTTTGAAGTCA GATAAACCGACCAGTACAG	This paper	N/A
wsc1$^{\Delta STR\Delta WSC}$ primer 5'forward to eliminate from +93 bp to +846 bp: GCATTCAAGGACGTATGGTTTGACATGT CAGCCGCCACCAACCGAGT	This paper	N/A
wsc1$^{\Delta TM}$ primer 5'forward to eliminate from +869 bp to +962 bp: TGCCGAGTCGCTCATTCTAATAGCGCTTG CATTCAAGGACGTATGGTT	This paper	N/A

(*Continued on next page*)

Please cite this article in press as: Neeli-Venkata et al., Detection of surface forces by the cell-wall mechanosensor Wsc1 in yeast, Developmental Cell (2021), https://doi.org/10.1016/j.devcel.2021.09.024

Continued

REAGENT or RESOURCE	SOURCE	IDENTIFIER
wsc1$^{\Delta CC}$ primer 5'forward to eliminate from +969 bp to +1098 bp: CAAATTTGTGACACGCAATATTCTAATT TTGAATCTCCTGAA	This paper	N/A
Recombinant DNA		
Vector: *pFA6a-mCherry-kanMX6*	Snaith et al., 2005	pKS390
Vector: pCR2.1-nat	Sato et al., 2005	NEG772014MC
Vector: pAL-*Wsc1-GFP:ura4+*	Cruz et al., 2013	pRZ21
Vector: pAL-*Wsc1*$^{\Delta WSC}$*-GFP:ura4+*	This paper	pRC22
Vector: pAL-*Wsc1*$^{\Delta STR}$*-GFP:ura4+*	This paper	pRC23
Vector: pAL-*Wsc1*$^{\Delta STR\ \Delta WSC}$*-GFP:ura4+*	This paper	pRC24
Vector: pAL-*Wsc1*$^{\Delta CC}$*-GFP:ura4+*	This paper	pRC25
Vector: *pFA6a-fus1*-3'UTR-AfeI-5'UTR-*kanMX*	Gift from S. Martin lab, Department of Fundamental Microbiology, University of Lausanne, Lausanne, Switzerland	pSM1966
Vector: *pFA6a-gap1*-3'UTR-AfeI-5'UTR-*hphMX*	Gift from S. Martin lab, Department of Fundamental Microbiology, University of Lausanne, Lausanne, Switzerland	pSM1869
Software and algorithms		
ImageJ	NIH	RRID: SCR_003070; https://imagej.nih.gov/ij/
Prism6	GraphPad	RRID: SCR_002798; https://www. graphpad.com/scientific-software/prism/
Photoshop CS6	Adobe	RRID: SCR_014199; https://www.adobe.com/downloads.html
MATLAB 2014a	The MathWorks, Inc.	RRID: nlx_153890; https://www.mathworks.com/
Metamorph	Molecular Devices	RRID: SCR_002368; https://www.moleculardevices.com/

RESOURCE AVAILABILITY

Lead contact

Further information and requests for resources and reagents should be directed to and will be fulfilled by the lead contact, Nicolas Minc (nicolas.minc@ijm.fr).

Materials availability

This study did not generate new unique reagents.

Data and code availability

- All data reported in this paper will be shared by the lead contact upon request
- This paper does not report original code.
- Any additional information required to reanalyze the data reported in this work paper is available from the lead contact upon request

Please cite this article in press as: Neeli-Venkata et al., Detection of surface forces by the cell-wall mechanosensor Wsc1 in yeast, Developmental Cell (2021), https://doi.org/10.1016/j.devcel.2021.09.024

EXPERIMENTAL MODEL AND SUBJECT DETAILS

Fission yeast strains and growth conditions

Standard *S. pombe* genetic procedures and media were used (Forsburg and Rhind, 2006; Moreno et al., 1991). The relevant genotypes and the source of the strains used are listed in Table S1. Genetic crosses and selection of the characters of interest was done by random spore analysis. All the deletions strains generated in this work were checked by PCR, drop assays with Caspofungin (0.5-1 μg/ml) when relevant, and growth on appropriate selection markers. For all microscopy experiments, unless otherwise indicated, liquid cultures were grown overnight in YE5S at 25°C, diluted in fresh medium and grown to an optical density (OD_{600}) between 0.4 and 0.6 before live-imaging.

METHOD DETAILS

Cloning and yeast genetics

(i) Wsc1-mCherry was obtained by tagging at its endogenous genomic locus at the 3′ end, yielding a C-terminally tagged protein. This was achieved by PCR amplification of a fragment from the template plasmid with primers carrying 5′ extensions corresponding to the last 80 nucleotides of the Wsc1 ORF and the first 80 nucleotides of the 3′UTR and integrated in the genome by homologous recombination (Bähler et al., 1998). The plasmid pVD11 (pFA6a-*mCherry-kanMX*) was used as a template for PCR with primers RN01 and RN02 as shown in key resources table and the resulting PCR product was transformed into a Wild-type (WT) h90 strain. The positive clones were selected on YE5S + 120 μg/mL Kan and the integration was confirmed by PCR.

(ii) Marker switching from Kan to Nat was achieved by amplifying the NatMX cassette from a pCR2.1-nat vector with primers MD1 and MD2 and transforming it into KanMX cassette-bearing strains (Haupt et al., 2018).

(iii) To generate *fus1Δ* and *gap1Δ* mutants expressing Wsc1-GFP, we used the plasmids pSM1966 (pFA6a-*fus1*-3'UTR-AfeI-5'UTR-*kanMX*) and pSM1869 (pFA6a-*gap1*-3'UTR-AfeI-5'UTR-*hphMX*) (kind gift from S. Martin, University of Lausanne, Switzerland). These plasmids were linearized with the restriction enzyme AfeI, purified, and transformed into a WT homothallic strain (RN42, h90). Positive clones were selected on YE5S + 120 μg/mL Kan or) YE5S + 300 μg/mL Hygromycin B plates and tested for functional and visual phenotypes.

(iv) Generation of Wsc1 alleles.

The mutated versions of Wsc1 were based on pAL-$wsc1^{+}$-GFP (pRZ21: Wsc1, fused with GFP at a *Not*I site on the C-terminal end carrying the $ura4^{+}$ marker at the 3′end (Cruz et al., 2013)). To generate Wsc1-GFP alleles, the plasmid pRZ21 was modified by site-directed mutagenesis using deletion loop oligonucleotides, listed in key resources table, to eliminate DNA base pairs (bp) from various positions, thus yielding $wsc1^{\Delta WSC}$-GFP (pRC22), $wsc1^{\Delta STR}$-GFP (pRC23), $wsc1^{\Delta STR\Delta WSC}$-GFP (pRC24),$wsc1^{\Delta TM}$-GFP (pRC42), and $wsc1^{\Delta CC}$-GFP (pRC25) vectors. From each of these plasmids, a *Spe*I-*Bgl*II fragment containing the mutagenized *wsc1* open reading frame (ORF) and flanking sequences were transformed into the wild type strain (SM215). Thus, each construct was present as a single copy in the cell under the control of the native *wsc1* promoter. To generate the untagged Wsc1 alleles, plasmids pRC22, pRC23, pRC24 and pRC25 were digested with the enzyme *Not*I to eliminate the GFP epitope. The genomic mutated alleles were tested by PCR to validate that they hold the right deletion and replace the wild-type allele. To obtain the untagged *wsc1* alleles ($wsc1^{\Delta WSC}$, $wsc1^{\Delta STR}$, $wsc1^{\Delta WSC\ \Delta STR}$ and $wsc1^{\Delta CC}$) in the $mtl2^{+}$ shut-off background, a cassette (*Spe*I-*Bgl*II fragment) for each *wsc1* deletion allele (untagged) was used to transform SC80 (*kan-P81xnmt1-*$mtl2^{+}$) cells carrying the $mtl2^{+}$ gene driven by the P81x*nmt1* promoter (Cruz et al., 2013).

(v) Generation of Mtl2-Wsc1 STR swap construct

GFP-Wsc1CC-Wsc1TMD-Mtl2STR-Wsc1CRD-Wsc1SS was based on pRZ21 ($wsc1^{+}$). pRZ21 was modified by site-directed mutagenesis by introducing two *Sal*I sites at positions +351 and +846 bp to eliminate the STR domain. To isolate the STR fragment from $mtl2^{+}$, pSC19 (Cruz et al., 2013) was mutagenized to create 2 *Sal*I sites at positions +105 and +702. Then the STR fragment from $mtl2^{+}$ (flanked by *Sal*I sites) was inserted in frame into pRZ21 cut with *Sal*I. As above, a *Spe*I-*Bgl*II fragment containing the hybrid *wsc1-STR-mtl2* was used to transform the wild type strain (SM215).

Mating assays

For mating assays, liquid cultures of homothallic strains were first grown in a minimum sporulation medium supplemented with Nitrogen (MSL+N) at 25°C until reaching an optical density (OD_{600}) between 0.5 and 1.0. On the second day, cultures were then diluted to an $OD_{600}\sim$ 0.025 in MSL+N and grown for 16-20h at 30°C to reach an $OD_{600}\sim$ 0.5-1.0. The third day, cells were washed thrice with MSL-N (without Nitrogen), and re-suspended to an $OD_{600}\sim$ 1.5 in 1 ml MSL-N and incubated at 30°C for 4-6h under agitation. Next, the cells were pelleted down by centrifugation, and 1 μl of cells were directly placed between an MSL-N agarose pads and a coverslip, followed by sealing with VALAP. The slide containing the cells were incubated for ~15h in a humidifled petri dish at 18°C. On the next day, microscopy images at different stages of mating were captured (Vjestica et al., 2016). For mating experiments between partners expressing different markers of the membrane, needed to compute apposed thickness of cell walls at sites of mating-tip contact, heterothallic strains of Wsc1-GFP (h-) and mCherry-Psy1 (h+) were grown in separate tubes as described above until the

Please cite this article in press as: Neeli-Venkata et al., Detection of surface forces by the cell-wall mechanosensor Wsc1 in yeast, Developmental Cell (2021), https://doi.org/10.1016/j.devcel.2021.09.024

second day. On the third day, an equal number of heterothallic partners were mixed, centrifuged and re-suspended in MSL-N medium. The next subsequent steps were similar as described above.

Micro-fabricated channels and microwells handling

The general design of microchannels to confine fission yeast cells ensured a near unlimited nutrient supply (Haupt et al., 2018), and were based on a 2-step soft-lithography protocole. A first thin layer of ~2.5 μm in height was first fabricated using SU8 photoresists, and subsequent UV illumination through a Quartz mask, and a subsequent second layer of ~40μm in height of SU8 photoresists, was spread on top of the first layer, and exposed with UV through a Quartz mask, aligned with the first design using a Mask Aligner. Poly-DimethylSiloxane (PDMS, Sylgard 184 from Dow Corning, Midland, Michigan, USA) replica were prepared at a 10:1 ratio of PDMS:curing agent. PDMS channels were covalently mounted onto 24x50 mm coverslips (VWR). To this aim, coverslips and PDMS replica were cleaned with Acetone, Isopropanol and ddH2O, dried with clean air, treated in a plasma cleaner (Harrick Scientific, USA) for 1min, placed on top of each other to become bound covalently, and baked at 65°C for ~1 hr.

For experiments using microchannels, cells were loaded as spores, which then germinated and proliferated as vegetative cells and crowded the microchannels (Haupt et al., 2018). Spores were obtained from homothallic h90 strains after placing freshly growing cells on solid ME medium plates at 25°C for 2-3 days. Mating mixtures were digested in 1/200 Glusulase (PerkinElmer, Waltham, Massachusetts, USA) at room temperature overnight, to eliminate vegetative cells. Digests were cleared of debris by adding four volumes of Percoll (Sigma-Aldrich) followed by centrifugation. Fresh spores were re-suspended in YE5S and pushed into channels by applying a pressure on the channel inlet with a syringe, usually yielding 1-6 spores per channel. The spore-containing channels were filled with YE5S and incubated for 16-18h in a humidified petri dish at 25°C. The next morning, channels were rinsed with fresh YE5S at least 1h before live-imaging.

For surface passivation of the microchannels, the channels were pre-treated with 2% pluronic acid (a non-ionic surfactant) dissolved in YE5S and left in the incubator for 1h at 37°C. A control (only YE5S) was also treated in a similar fashion. Spores were subsequently loaded into both of these channels. In comparison to control, spores in the pluronic acid treated channels tended to flow out of channels much easily, suggesting that non-specific adhesion was well suppressed.

For temperature sensitive alleles, *cwg1-1*, *orb6-25*, and *sec8-1* spores were grown in channels at permissive temperature (25°C) overnight, rinsed with fresh media the next morning and then switched to restrictive temperature (36°C) for 6h, 2h, and 1h respectively, before observation. For sorbitol treatments, cells were grown in microchannels in YE5S medium as above, and subsequently rinsed with large volumes of YE5S + 2 M Sorbitol, to ensure fast medium exchange. To compute the thickness of apposed cell walls at sites of cell contacts in microchannels an equal volume of Wsc1-GFP and mCherry-Psy1 expressing spores were mixed and pushed into the channels. These channels were filled with YE5S and incubated for 16-18h at 25°C.

Rounded PDMS micro-wells were fabricated from a template of micro-fabricated posts in SU8 using soft-lithography, as described above (Minc et al., 2009a, 2009b). PDMS slabs containing thousands of wells of sizes ranging from 10-25μm in diameter were first vacuumed for 20 min and incubated in YE5S for ~ 1h before being treated with a Plasma Cleaner to render them hydrophilic. Cells were pelleted and a 1-2 μl drop was placed on top of the wells and covered by a coverslip. PDMS chambers were surrounded by humid kim-wipes to limit evaporation. Cells that had fallen into a micro-well were filmed immediately.

Pharmacological inhibition

The microtubule -depolymerizing drug Methyl 2-Benzimidazole Carbamate (Carbendazim, MBC) (Sigma-Aldrich, St. Louis, Missouri, USA) was used at a final concentration of 25 μg/ml from a 2.5 mg/ml stock dissolved in DMSO (Euromedex, Souffelweyersheim, France) The addition of chemical during imaging was performed by perfusing large amount of YE5S medium containing either MBC or DMSO (for controls) in microchannels. Caspofungin (Sigma-Aldrich) was used at a final concentration of 0.5 μg/ml, from a 5 mg/ml stock. Caspofungin was added to agar pads.

Turgor pressure manipulation using various sorbitol doses

To assess the turgor pressure values required to maintain Wsc1 clusters, various sorbitol doses ranging from (0.25 M – 2 M dissolved in YE5S) were tested. First, 2 pre-images of WT cells in microchannels were acquired followed by the rapid addition of large volumes of YE5S supplemented with sorbitol into the channel inlets. Post-sorbitol images were acquired within 5 minutes of rinsing and filmed subsequently.

Cell death assays

For cell death assay experiments using untagged Wsc1 alleles, homothallic strains were either grown in microchannels or in liquid cultures in YE5S medium. Cells grown in liquid cultures, were placed on an agarose pad, and imaged within 1h, and cell death was quantified visually. For microchannel assays, cells were grown to a high confinement, assayed from the appearance of miss-shaped cells, and cell death was quantified visually. For cell death assay experiments using untagged Wsc1 alleles in an Mtl2-shutoff background under the control of the P81x*nmt1* promoter, liquid cultures were grown overnight in Edinburgh Minimal Medium supplemented with amino acids at 25°C. The next morning, 2 ml of this overnight culture was pelleted and diluted in Edinburgh Minimal Medium supplemented with amino acids and with 5 μg/ml of thiamine with a starting OD_{600} ~ 0.05-0.1. The cells were left in the incubator at 25°C for ~9h before imaging.

Please cite this article in press as: Neeli-Venkata et al., Detection of surface forces by the cell-wall mechanosensor Wsc1 in yeast, Developmental Cell (2021), https://doi.org/10.1016/j.devcel.2021.09.024

Microscopy

All live-cell imaging experiments were performed on YE5S 2%-agarose pads, or MSL-N 2% agarose pads (for mating) or in microchannels and microwells. All images and time lapses presented throughout this work are single spinning disk confocal mid-sections to provide a true representation of Wsc1-GFP dynamics. We note this is different than merged stacks presented in (Cruz et al., 2013). Imaging was carried out at room temperature (22–25°C) on an inverted spinning-disk confocal microscope equipped with a motorized stage and an automatic focus (Ti-Eclipse, Nikon, Japan), a Yokogawa CSUX1FW spinning unit, and an EM-CCD camera (ImagEM-1K, Hamamatsu Photonics, Japan), or a Prime BSI camera (Photometrics). Images were acquired with a 100X oil-immersion objective (CFI Plan Apo DM 100X/1.4 NA, Nikon) in combination with a 2.5X magnifying lens. For laser ablation assays, we used an iLas2 module (GATACA Systems, France) in the ''Mosquito'' mode, irradiating cells at diffraction-limited spot with a 355 nm laser with a 60X oil-immersion objective (CFI Apochromat 60X Oil λS, 1.4 NA, Nikon), and the subsequent images were captured using a 100X oil-immersion objective. The microscope was operated with the Metamorph software (Molecular Devices).

Fluorescence Recovery after Photobleaching (FRAP) was performed using the iLas2 module (GATACA Systems, France) on the spinning disk confocal system described above. A 0.5 μm circular ROI was bleached following two pre-bleach acquisitions and recovery was followed for every 30-second interval. Other shorter or longer time-intervals were also assayed as preliminary trials to optimize this analysis and identify the proper timescale to quantify Wsc1 motility.

Cell death assays were performed on a wide-field fluorescence microscope (TI-Eclipse; Nikon) operated with Micro-Manager (Open Imaging). Cells were imaged with a 100X objective in DIC (Differential Interface Contrast) which allows to clearly distinguishing dead from live cells.

QUANTIFICATION AND STATISTICAL ANALYSIS

Image analysis and quantifications

To quantify local fluorescent enrichment, a semi-automated homemade Matlab (Mathworks) script was developed. The script removes fluorescent background and allows the user to trace a line manually around the cell contour, visible from Wsc1-GFP or other marker's signals, around cell tips, or cell sides. The line scan typically span the site of contact and cell sides with no contact, along a distance of 5-7μm (see Figure 1B as a representative example). The fluorescence was averaged on a thickness of 14px across the membrane (for a pixel size of 43.1nm), in order to average signals from both cells at sites of cell contacts, and fitted with a Gaussian, to extract basal fluorescent levels away from clusters, and the maximum signal in clusters. The ratio between max and min was used to compute enrichment . In order to compare Wsc1 enrichment, at a contact between two cells, with that in a free cell tips, or to a contact formed with a neighbor expressing a protein tagged in another color, the scripts was modified in the latter cases to a thickness contour of 7 px, and the enrichment was multiplied by a factor 2 for normalization. Finally, cluster sizes was quantified as the full width at mid-height of the Gaussian fit of Wsc1 signal along the local contour.

FRAP data were analyzed, by computing the fluorescence recovery in the bleached region, after background subtraction, and was normalized to the signal of 3 unbleached regions of interest in cells in the same field, to account for photobleaching. Each recovery curve was fitted with a single exponential, to extract individual half-times and mobile fractions. The data were also averaged to plot mean recovery dynamics presented in Figure 6A. To estimate a 2D diffusion coefficient from the half-times, we assumed that diffusion occurred in 2D in the membrane plane, and used formula derived in (Kang et al., 2012).

Cell wall thickness measurements initiates with a two-color mid-slice confocal image, and traces segments perpendicular to the membrane, to detect the local distance between the two Gaussian peaks. Upon image registration, obtained by calibrating the field with multi-spectral beads scanned around the field of view, the distance is corrected and computed to extract local thickness. The impact of differences in signal intensities are automatically corrected to extract the true signal peak by using an analytical expression of the convoluted intensity profile (Davì et al., 2018, 2019). Thicknesses of apposed cell walls were averaged around the center of the zone of cell contacts where clusters formed.

Statistical Analysis

All experiments presented in this MS were repeated at least twice and quantified in a number of cells or events detailed in each figure legend. Statistical and correlation analyses were carried out using Prism 6 (GraphPad Software, La Jolla, CA). To compute significance throughout this work, we used a two-tailed non-parametric Mann-Whitney test. Statistically significant differences are reported in figure legends.